Comparison of model electron densities and temperatures with Millstone Hill observations during undisturbed periods and the geomagnetic storms of 16–23 March and 6–12 April 1990

A. V. Pavlov[1,2] **M. J. Buonsanto**[2]

[1] Institute of Terrestrial Magnetism, Ionosphere and Radio-Wave Propagation, Russia Academy of Science (IZMIRAN), Troitsk, Moscow Region, 142092, Russia
[2] Haystack Observatory, Massachusetts Institute of Technology, Westford, Mass., USA

Abstract. Measurements of F-region electron density and temperature at Millstone Hill are compared with results from the IZMIRAN time-dependent mathematical model of the Earth's ionosphere and plasmasphere during the periods 16–23 March and 6–12 April 1990. Each of these two periods included geomagnetically quiet intervals followed by major storms. Satisfactory agreement between the model and the data is obtained during the quiet intervals, provided that the recombination rate of $O^+(^4S)$ ions was decreased by a factor of 1.5 at all altitudes during the nighttime periods 17–18 March, 19–20 March, 6–8 April and 8–9 April in order to increase the NmF2 at night better to match observations. Good model/data agreement is also obtained during the storm periods when vibrationally excited N_2 brings about factor-of-2-4 reductions in daytime NmF2. Model calculations are carried out using different expressions for the $O^+ - O$ collision frequency for momentum transfer, and the best agreement between the electron-density measurements and the model results is obtained when the CEDAR interim standard formula for the $O^+ - O$ collision frequency is used. Deviations from the Boltzmann distribution for the first five vibrational levels of N_2 were calculated. The calculated distribution is highly non-Boltzmann at vibrational levels $j > 2$, and the Boltzmann distribution assumption results in the increase of 10–30% in calculated NmF2 during the storm-time periods. During the March storm at solar maximum the model results obtained using the EUVAC solar flux model agree a little better with the observations in comparison with the EUV94 solar flux model. For the April storm period of moderate solar activity the EUV94X model results agree better with the observations in comparison to the EUVAC model.

Correspondence to: A. V. Pavlov

1 Introduction

There are many physical models of electron density, N_e, in the F region of the ionosphere. These models solve the ion and electron continuity, momentum, and energy equations and have the capability to predict day-to-day variability of the ionosphere. The large uncertainties in the calculated neutral winds lead to errors in the plasma drift and, as a result, to errors in the calculated peak height of the F2 layer (hmF2). This problem was largely overcome when Buonsanto (1986), Miller *et al.* (1986), and Richards (1991) develped a technique for deriving equivalent neutral winds from the observed hmF2. This method with some modification is used in our model to carry out a comprehensive study of the response of the ionosphere to the March and April 1990 geomagnetic storms. These modeled results are compared with the data (Buonsanto *et al.*, 1992a) and with ionospheric densities and temperatures calculated using the measured neutral winds and electric fields given by Buonsanto *et al.* (1992a) as input parameters for our theoretical model. However, we often do not have the observed hmF2, and the problem of uncertainties in the calculated neutral winds arises again. In this case we can use the IRI hmF2, (Bilitza, 1990) to avoid some errors in the electron density during magnetic storms (Pavlov, 1996). In this paper, we use this new approach for the March and April 1990 geomagnetic storms (Buonsanto *et al.*, 1992a) to estimate the inaccuracies in the prediction of the modeled NmF2 and hmF2. We compare our results and conclusions with modeling results given by Richards *et al.* (1994b) for the March 1990 magnetic storm.

The resonant charge transfer interaction between O^+ and O is of great importance in ionospheric modeling (Moffett *et al.*, 1990). Uncertainties in their crossections give inaccurate values for the momentum transfer collision frequency of $O^+ - O$. The commonly accepted value of the $O^+ - O$ frequency is given by Banks (1966) as

$$v_{in}(B) = 3.5 \cdot 10^{-17} \, T^{0.5} \, (1 - 0.065 \log T)^2 \, [O], \qquad (1)$$

where $T = (T_i + T_n)/2$.

The most recent theoretical developments of this ion-neutral collision frequency can be represented (Pesnell *et al.*, 1993) by

$$v_{in}(P) = 5.9 \cdot 10^{-17} \, T^{0.5} \, (1 - 0.096 \log T)^2 \, [O] \cdot \qquad (2)$$

From indirect measurements of this frequency it follows that the value of $v_{in}(B)$ must be increased by factor 1.2–2.4 (Burnside *et al.*, 1987; Sipler *et al.*, 1991., Buonsanto *et al.*, 1992b; Reddy *et al.*,1994; Davis *et al.*, 1995). The recommended interim standard for momentum transfer collision frequency of $O^+ - O$ adopted at the 1992 CEDAR meeting is given by Salah (1993) as

$$v_{in}(S) = 4 \cdot 10^{-17} \, T^{0.5} \, [O]. \qquad (3)$$

The difference between $v_{in}(P)$ and $v_{in}(S)$ is not only in the number coefficient but also in the temperature dependence of this frequency. In this paper, we examine which collision-frequency formula, that of Banks (1966), Pesnell *et al.* (1993), or Salah (1993) can produce the best agreement between observed and predicted values of NmF2 and hmF2 at Millstone Hill.

The March and April 1990 geomagnetic storms were at solar maximum and moderate solar-activity conditions when the vibrationally excited nitrogen played an important role in the ionosphere (Torr and Torr, 1982; Pavlov, 1988; Richards and Torr, 1986; Pavlov, 1994). That is why it is important to investigate the role of the vibrationally excited nitrogen in producing the negative phases of these ionospheric storms.

In earlier studies, Newton *et al.* (1974) and Pavlov (1989) found that deviation from a Boltzmann distribution of $N_2(v)$ was large in the SAR-arc region at the vibrational energy levels $v > 2$, and this deviation significantly affected the loss rate, L, of the $O^+(^4S)$ ions at F2-region altitudes. Torr and Torr (1982) calculated a vibrational distribution of $N_2(v)$ during undisturbed conditions at middle latitudes. Richards *et al.* (1986) studied the effects of the vibrationally excited nitrogen on the electron temperature, T_e, during quiet periods for a non-Boltzmann distribution of $N_2(v)$. Pavlov and Namgaladze (1988) calculated a vibrational distribution of $N_2(v)$ and found that the difference between the Boltzmann and non-Boltzmann distribution of $N_2(v)$ does not have any effect on the electron density and temperature at solar minimum. Previous work concerning the role played by vibrationally excited molecular nitrogen in the formation of the disturbed F-region electron density and temperature have assumed a Boltzmann distribution of $N_2(v)$. In this paper we will examine the effect of a non-Boltzmann distribution of $N_2(v)$ on the electron density and temperature during geomagnetic storms.

Large, short-lived electric fields are often observed in the mid-latitude trough (Rodger *et al.*, 1992). The perpendicular electric fields $E_\perp$ (with respect to the magnetic field) produce significant effects in N_e and the ion temperature, T_i (Schunk *et al.*, 1975; Raitt *et al.*, 1976). These changes in the electron density and ion temperature are the reason for the electron-temperature disturbances. These electric fields were stronger during the April 1990 storm than during the March 1990 storm at Millstone Hill (Buonsanto *et al.*, 1992a). During the day on 10 April 1990, extremely low values of hmF2 < 200 km (indicating an F1 peak due to molecular ions) and high ion velocities in excess of 500 ms^{-1} were observed above Millstone Hill (Buonsanto *et al.*, 1992a). These could be due to the perpendicular electric fields. An important aim of this paper is to study the effects of these $E_\perp$ on N_e. Our task is also to estimate the values of these electric fields needed to produce agreement between the measured and calculated hmF2 and the measured and calculated ion temperatures during the day on 10, April 1990 and to compare these electric fields with the measured electric fields given by Buonsanto *et al.* (1992a).

By using a theoretical model we can forecast the values of NmF2 and hmF2 during magnetic storms. Such predictions of NmF2 and hmF2 are also possible to carry out using the semiempirical IRI approach described by Kishcha (1995). During geomagnetic storms and substorms this analytical approach gives deviations of NmF2 and hmF2 from quiet condition values of NmF2 and hmF2. We also compare the accuracy of the theoretical and semiempirical IRI approach.

2 IZMIRAN model

The model of the thermal plasma in the ionosphere and plasmasphere used in the present study is described in detail by Pavlov (1994), and hence only a brief description will be given here. The IZMIRAN model is a one-dimensional model that uses a titled dipole approximation to the Earth's magnetic field and takes into account the difference between geographic and magnetic axes. In the model, coupled time-dependent equations of continuity, momentum, and energy balance for $O^+(^4S)$ and H^+ ions and electrons, are solved along a centered-dipole magnetic field line for the concentrations, field-aligned diffusion velocities, and temperatures of ions and electrons from a base altitude (160 km in the present study) in the northern hemisphere through the plasmasphere to the same base altitude in the southern hemisphere. Electron heating due to photoelectrons is provided by a solution of the Boltzmann equation for photoelectron flux along the entire flux tube using the method of Krinberg and Tashchilin (1984) on the same field-line grid used in solving the densities and temperatures. In the northern and southern hemispheres the IZMIRAN model solves time-dependent continuity equations for $O^+(^2D)$, $O^+(^2P)$, $O(^1D)$ vibrationally excited nitrogen quanta, and the momentum equations for the horizontal components of thermospheric wind within the altitude range 120–700 km and time-dependent continuity equations for NO^+, O_2^+, and N_2^+

ions in the region between 120 and 500 km in altitude. In order to take into account the strong dependence of the $O^+(^4S) + N_2 \rightarrow NO^+ + N$ reaction rate on vibrational excitation of N_2 (Schmeltekopf et al., 1968; Van Zandt and O' Malley, 1973; Pavlov, 1988) the number densities of excited molecular nitrogen at the first five vibrational levels are determined from the Boltzmann distribution using the calculated vibrationally excited nitrogen quanta. In the photochemical scheme described by Pavlov (1994) we changed the rate coefficients of the reactions of $O^+(^2P)$ with N_2 and O as recommended by Chang et al. (1993). To calculate more exactly the electron temperature from the electron-energy equation, we used the approximation to the multicomponent electron thermal conductivity coefficient given by Pavlov (1996). The model includes the option to use the models of the $O^+ - O$ collision frequency given by Banks (1966), Pesnell (1993), and Salah (1993).

The distribution of ionization in the topside ionosphere and plasmasphere is strongly controlled by the geomagnetic field, and therefore the IZMIRAN model calculations are valid up to $L \approx 6$ (L is the shell value of the geomagnetic field) where the geomagnetic field is close to the dipole approximation (Krinberg and Tashchilin, 1984). The model cannot give a correct description of the ionosphere between $-20°$ and $20°$ magnetic latitude, which would require taking into account the exchange by ions and electrons between all magnetic tubes because of the action of electromagnetic drift.

The three key inputs to the IZMIRAN model are the concentrations and temperature of the neutral constituents, the solar EUV fluxes, and the plasma drift velocity. To simulate the magnetic-storm effects on the neutral atmosphere, the MSIS-86 model (Hedin, 1987) was run using the 3-h A_p indices, while the solar EUV fluxes are from the EUVAC model (Richards et al., 1994a) or EUV94X model (Tobiska, 1993, 1994). To maintain the model nighttime E and Fl regions of the ionosphere, the simple approach to describe the neutral ionization by scattered solar 121.6-, 102.6-, and 58.4-nm radiation fluxes is used (Kashirin, 1986). The large uncertainties in the plasma drift velocity lead to errors in the calculated peak height of the F2 layer. Therefore, in the northern hemisphere, instead of calculating thermospheric wind components by solving the momentum equations given by Pavlov (1994), we use the approach developed by Richards (1991) to calculate an equivalent neutral wind from the hmF2 measurements given by Buonsanto et al. (1992a). Our implementation of the Richards (1991) method is explained in Appendix A. For the March and April 1990 magnetic storms we also use the measured neutral winds and electric fields given-by Buonsanto et al. (1992a) as input parameters for our theoretical model. The major enhancement to the IZMIRAN model described by Pavlov (1994) is the inclusion of electric-field effects on N_e and T_i in the frame of the one-dimensional IZMIRAN model as described by Pavlov (1996). Finally, the new approach given by Pavlov (1996) is applied to estimate the errors in NmF2 and hmF2 for the geomagnetic storms when the observed hmF2 are unavailable.

3 Undisturbed period and storms of 16–23 March 1990

The undisturbed period of 16–17 March 1990 (A_p of 8 and 3) and the 18–23 March 1990 magnetic storms (A_p between 14 and 73) occurred at solar maximum where the 10.7-cm solar flux increased from 180 on 16 March to 247 on 23 March. During 18–23 March 1990 two geomagnetic storms took place: a minor storm with a gradual commencement time near 0400 UT on 18 March and a major storm with a sudden commencement time near 2245 UT on 20 March. The data used in this paper (the variations of electron density and temperature) were taken by the incoherent-scatter radar at Millstone Hill, Massachusetts (Buonsanto et al., 1992a).

Figure 1 is a plot of the measured hmF2 and NmF2 for the period 16–23 March 1990 and the model results with and without effects of vibrationally excited N_2 included in the calculated $O^+(^4S)$ recombination rate
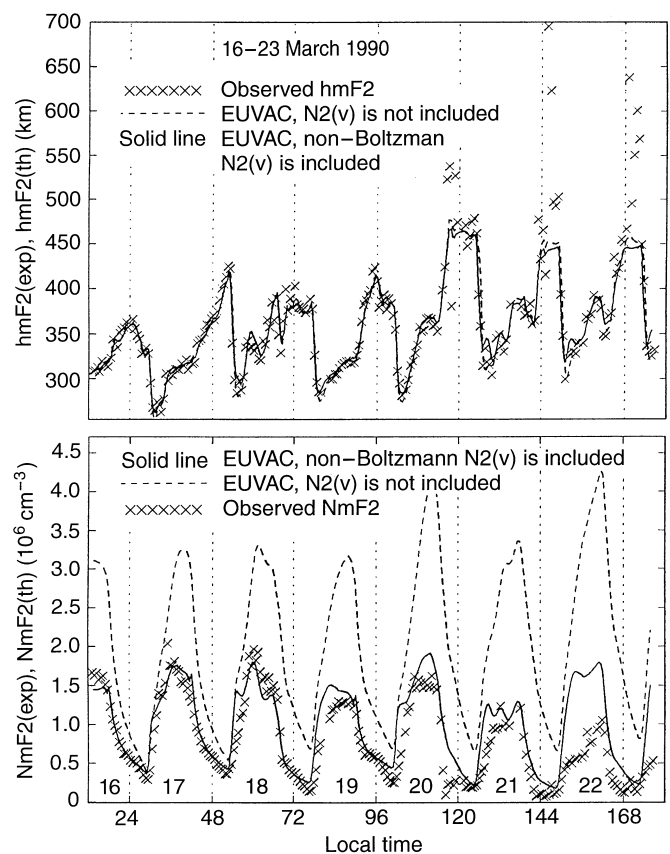

Fig. 1. Observed (*crosses*) and calculated F2 peak parameters above Millstone Hill for 16–23 March 1990. (Top) hmF2. (Bottom) NMF2. The solid lines are hmF2 and NmF2 from the IZMIRAN model when the non-Boltzmann populations of the first five vibrational levels of $N_2(v)$ are included in the calculated $O^+(^4S)$ recombination rate, and this recombination rate was decreased by the factor 1.5 during the nighttime periods of 16–18 and 19–20 March with solar zenith angles more than $90°$, and *dashed lines* are hmF2 and NmF2 when $N_2(v)$ is not included in the calculations with the original $O^+(^4S)$ recombination rate. The EUVAC solar flux model, the method of Eqs. A.18, A.20 for obtaining equivalent neutral winds from the height of the F2 peak electron density, and the $O^+ - O$ collision frequency given by Salah (1993) were used in the IZMIRAN model

which will be explained later. There are clear negative and positive phases in NmF2 compared to the undisturbed NmF2 on 17 March with the largest negative phase near 2030 LT on 20 March.

3.1 Uncertainties in the collision frequency of O^+–O and the loss rate of the $O^+(^4S)$ ions

The uncertainties associated with the O^+–O collision crossection give the uncertainty in the O^+–O collision frequency. In this paper, we use two theoretical approaches given by Eqs. 1 and 2 (Banks, 1966, and Pesnell, 1993, respectively) and Eq. 3, the CEDAR interim standard for the O^+–O frequency (Salah, 1993). The O^+–O frequency given by Pesnell (1993) is larger than that given by Banks (1966) and less than that given by Salah (1993). Solid and dashed lines of Fig. 2 give the comparison of the modeled densities using two different
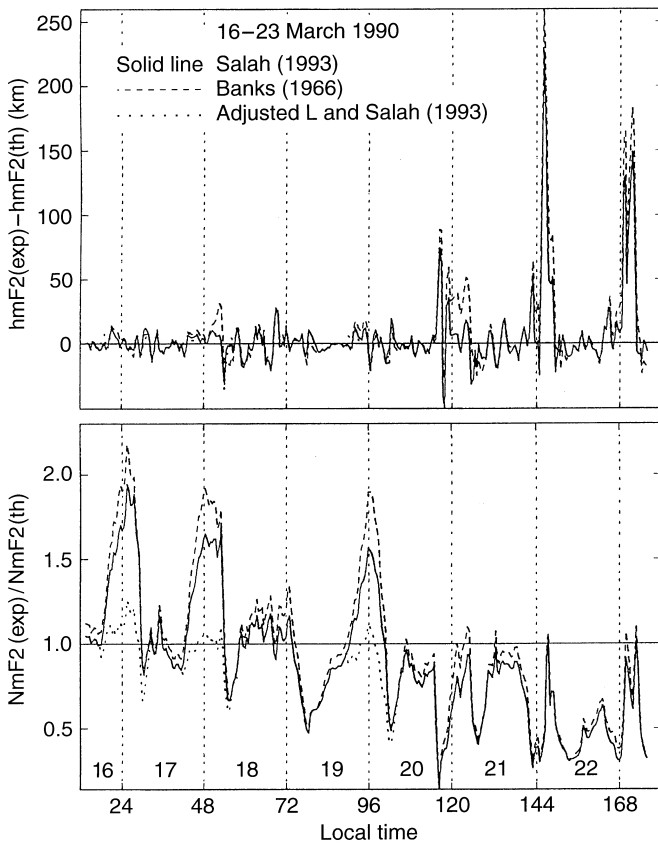

Fig. 2. (*Top*) Differences between the measured hmF2(exp) and the modeled hmF2(th), and ratios of the measured NmF2(exp) to the modeled NmF2(th) (*bottom*) for the magnetically quiet and disturbed periods of 16–23 March 1990 for the EUVAC solar flux model. The model results were obtained using the method of Eqs. A.18, A.20 for obtaining equivalent neutral winds from the height of the F2 peak electron density with the original $O^+(^4S)$ recombination rate (*solid and dashed lines*) and when this recombination rate was decreased by the factor 1.5 during the nighttime periods 16–18 and 19–20 March with solar zenith angles more than 90° (*dotted lines*). The O^+ –O collision frequencies given by Salah (1993) (*solid and dotted lines*) and Banks (1966) (*dashed lines*) were used in the IZMIRAN model

assumptions Eqs. 1 and 3. We can see that the O^+–O frequency of Salah (1993) gives the best agreement between measured and modeled NmF2. The method based on the Richards (1991) approach (Eqs. A.18, A.20) will naturally mimic the measured hmF2 during the quiet and disturbed periods on 16–21 March. Significant errors in the calculated hmF2 during 22 and 23 March are the result of the rapid fluctuations in the measured hmF2. There is the excellent agreement between the modeled NmF2 and the data on days 16–18. During 16–19 March the disagreement between measured and modeled NmF2 is not more than a factor of 2.

The results of Fig. 2 show that the use of the frequency given by Banks (1966) leads to a 5–10% decrease in the calculated daytime NmF2 and up to about 25% at night in comparison with NmF2 calculated by using the frequency given by Salah (1993). In order to illustrate the basic physics involved and to find out the physical reasons of this nighttime difference (but not for calculations) it is useful to use the analytical description of the nighttime NmF2 given by Krinberg and Tashchilin (1982, 1984):

$$NmF2(t) \approx NmF2(t_0) \exp[-(t - t_0)L(t)] + 3F_\infty(t)T_n(t)v_{in}(t)/[T_i(t) + T_e(t)]/g, \quad (4)$$

where

$$L = \sum_{j=0}^{5} k_j [N_2 (j)] + \gamma[O_2], \quad (5)$$

k_j and γ are the recombination rate coefficients of $O^+(^4S)$ ions with N_2 ($j = 0$–5) and O_2, $NmF2(t_0)$ is the ionospheric electron density for the local time t_0 corresponding to dusk, T_n is the exospheric neutral temperature, T_j and T_e are ion and electron temperatures, g is the acceleration due to gravity, v_{in} is the O^+– O collision frequency, F_∞ is the value of plasma ion flux flowing from the plasmasphere into the ionosphere, the values of L, T_i, T_e, g and v_{in} are chosen at the F2-peak altitude.

We can see from (4) that the nighttime F2-region electron density consists of two parts. The first term describes the role of the daytime ionization in the maintenance of the nighttime ionosphere. In this case the F region would decay with the characteristic time $\sim L^{-1}$ (~several hours). The nocturnal F region is also maintained by a downward flow of ionization from the plasmasphere described by the second term in Eq. 4. In winter, in spring, and in autumn, when the night is long enough, the role of the second term in Eq. 4 increases before sunrise and this term determines NmF2 as a function of v_{in}.

It seems likely that the nighttime discrepancy between measured and modeled NmF2 is caused by inaccuracies in key inputs, such as the composition and temperature of the neutral atmosphere (the MSIS-86 model does not accurately predict the neutral atmosphere during the quiet period and the magnetic storm), and the recombination rate coefficients of $O^+(^4S)$ ions with N_2 ($j = 0$–5) and O_2.

Dotted lines on Fig. 2 show the model results when the recombination rate of the $O^+(^4S)$ ions was decreased by a factor of 1.5 by decreasing the MSIS-86 N_2 and O_2 densities by 1.5 at all altitudes during the nighttime 16–18 March and 19–20 periods when the solar zenith angle was more than $90°$ in the northern hemisphere. No adjustments were made to the L values at any other times. This recombination rate adjustment is sufficient in order to reproduce very well the observed nighttime NmF2 on 17–18 March and 19–20 March.

As Fig. 2 shows, there is large disagreement between the measured and modeled NmF2 on 22–23 March. The F region was depleted during this time period, as the main ionospheric trough moved equatorward of Millstone Hill (Buonsanto *et al.*, 1992a). Enhanced sunward convection (500–1700 m s^{-1}) was observed on 22 March. These large ion drift velocities are the subauroral ion drift phenomenon (Foster *et al.*, 1994), and therefore we can assume these drifts were connected with large, short-lived electric fields (∼ up to 1–3 h) often observed in the mid-latitude trough (Rodger *et al.*, 1992). These electric fields can have important effects on N_e and the ion temperature. The rate coefficients of such important ionospheric processes as the reactions of $O^+(^4S)$ with N_2 and O_2 depend on the effective temperature, which is a function of the ion temperature, the neutral temperature, and the plasma drift velocity (Albritton *et al.*, 1977; St.-Maurice and Torr, 1978). These effects are not taken into account in the model used here, giving the mentioned disagreement between the measured and calculated NmF2. Some results of these effects of electric fields on the electron density are presented in Sect. 5.

3.2 Vibrationally excited nitrogen

In the IZMIRAN model, the number densities, n_j, of excited molecular nitrogen $N_2(j)$ at the vibrational level, j, are determined from the Boltzmann distribution

$$n_{jB} = n_{0B} \left[\alpha/(1 + \alpha)\right]^j = n_{0B} \exp(-jT_v), \qquad (6)$$

where α is the vibrational quanta and T_v is the vibrational temperature. In this case, from Eq. 6 follows that the sum of the vibrationally unexcited and excited molecular nitrogen concentrations (Pavlov and Namgaladze, 1988):

$$[N_2] = n_{0B} (1 + \alpha). \qquad (7)$$

There is no possibility to differentiate the vibrationally unexcited N_2 from the vibrationally excited N_2 during the mass-spectrometer measurements of the neutral species in the atmosphere, and therefore we believe that the MSIS-86 model calculates the value of $[N_2]$. The difference between $[N_2]$ and n_{0B} is not negligible for the March 1990 magnetic storm. For example $[N_2] /n_{0B} = 1.12$ for $T_v = 1500$ K.

The ability of the IZMIRAN model to reproduce the measured NmF2 is illustrated in Fig. 3. The solid line is a model result when the vibrationally excited nitrogen is included in the calculations of the loss rate L of the $O^+(^4S)$ ions as determined by Eq. 5. The dashed lines in Figs. 1 and 3 are model results when the vibrationally excited nitrogen is not included in the calculations of L with $k_j(j > 0) = 0$ and $L = k_0 [N_2]/(1 + \alpha) + \gamma[O_2]$. The approach based on the Richards (1991) method (Eqs. A.18, A.20) for obtaining equivalent neutral winds from the height of the F2 peak electron density and the O^+–O frequencies given by Salah (1993) were applied to the model. From Figs. 1 and 3 it follows that there is a large increase in the modeled NmF2 without the vibrationally excited nitrogen and the model densities are unreliable. Both the daytime and nighttime densities are not reproduced by the model without the vibrationally excited nitrogen. Inclusion of vibrationally excited N_2 brings the model and data into agreement. The increase in the $O^+ + N_2$ rate factor due to the vibrationally excited nitrogen produces factors of 2–4 reductions in the daytime peak density. The effect of vibrationally excited N_2 on N_e is most pronounced during the daytime.
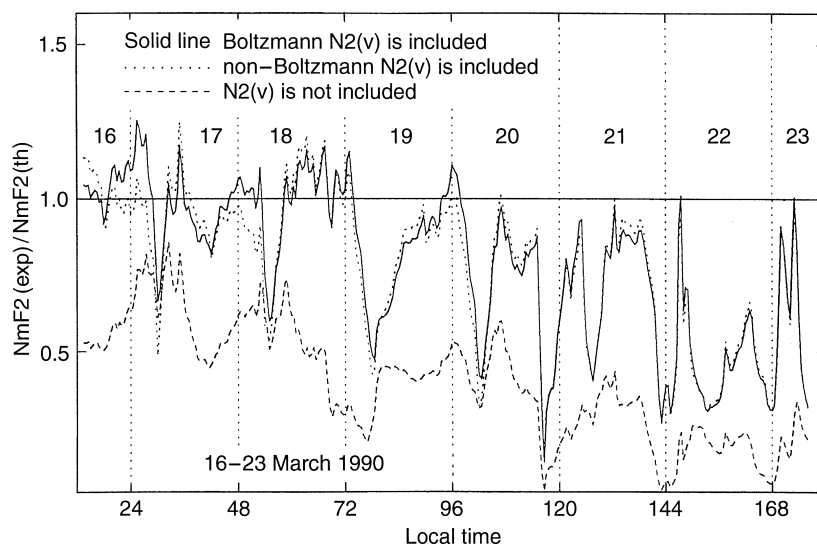

Fig. 3. Ratios of the measured F2 peak densities NmF2(exp) to the modeled F2 peak densities NmF2(th) during the 16–23 March 1990 period for the EUVAC solar flux model. The modeled NmF2 were obtained using the Boltzmann vibrational distribution of $N_2(v)$(*solid line*) and the non-Boltzmann populations of the first five vibrational levels by solving the $N_2(v = 1–5)$ time-dependent continuity equations (*dotted line*), and when $N_2(v)$ was not included in the calculations (*dashed line*). The original $O^+(^4S)$ recombination rate was decreased by the factor 1.5 during the nighttime periods 16–18 and 19–20 March and the $O^+ - O$ collision frequencies given by Salah (1993) were used in the IZMIRAN model

3.3 Non-Boltzmann distribution of vibrationally excited molecular nitrogen

There are some deviations of n_j from n_{jB} in the F region of the ionosphere (Newton *et al.*, 1974; Torr and Torr, 1982; Richards *et al.*, 1986; Pavlov, 1988, 1989, Pavlov and Namgaladze, 1988). These deviations can affect the recombination rate of $O^+(^4S)$ ions and the heating rate of electrons due to the de-excitation reactions of excited molecular nitrogen. In order to study the possible effects of deviations of n_j from n_{jB} on the electron temperature and density let us consider the model description of excited molecular nitrogen.

Pavlov (1988, 1989) treated the vibrationally excited nitrogen molecule as a set of harmonic and anharmonic oscillator energy levels. The Pavlov (1989) study suggests that the effect of anharmonicity on n_j is small at the energy levels, $j = 1–5$. Therefore our model used the system of Eqs. 15–18 given by Pavlov (1988) to determine $n_j(j = 1–5)$ using the harmonic oscillator energy level approximation, the vibrational-vibrational and vibrational-translational energy exchange of $N_2(j)$, the diffusion of $N_2(j)$ in the mixture of $N_2(0)$, O_2, and O, and the production rates of $N_2(j)$ by thermal electron excitation of N_2 (0), and by the reactions $O(^1D)$ with N_2 (0) and $N(^4S)$ with NO. This system of equations is numerically integrated within the altitude range 120–700 km in the northern and southern hemispheres. At the lower boundary the diffusion processes of vibrationally excited molecules were neglected. The upper-boundary conditions are zero fluxes for all excited levels. In order to calculate the value of n_5 it is required to know the value of n_6. By analogy with the Boltzmann distribution the condition $n_6/n_5 = n_5/n_4$ was assumed.

The results of calculating n_j/n_{jB}, and T_n are presented in Fig. 4. The present study suggests that the calculated distribution is highly non-Boltzmann at the vibrational levels $j > 2$ just after sunrise. The deviations from the Boltzmann distribution are not significant at the first and second vibrational levels of N_2. These relative deviations increase with level number and approach factors of 6 and 38 for the third and the fourth excited levels. The deviations n_3/n_{3B} and n_4/n_{4B} have their maximum values during the period 6.30–7.30 LT. From the diurnal variations of the calculated vibrational (solid line) and neutral (dashed line) temperatures shown in Fig. 4 it follows that $T_v < T_n$ is realized in the atmosphere for the nighttime periods where the produc-

tion frequency of N_2 (j) is low (details are given by Pavlov, 1994). This means that for these periods the populations of $N_2(j)$ are less than the populations for a
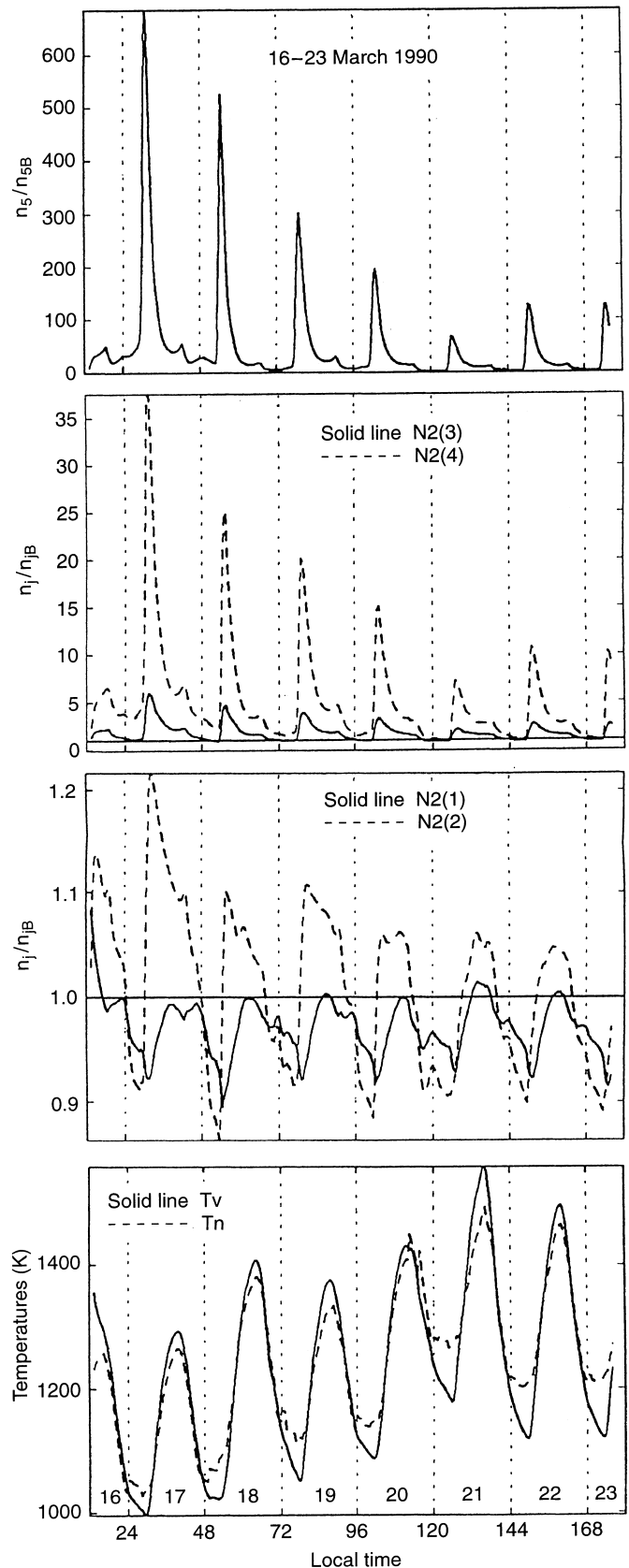

Fig. 4. The time variations of the vibrational and neutral temperatures and populations of the first five vibrational levels of N_2 in comparison with the Boltzmann distribution during the 16–23 March period at the F2 peak altitude. The *solid lines* show the modeled T_v, n_1/n_{1B}, n_3/n_{3B}, and n_5/n_{5B} and the *dashed lines* show the modeled T_n, n_2/n_{2B}, and n_4/n_{4B}. The $O^+ - O$ frequencies given by Salah (1993) and the approach of Eqs. A.18, A.20 based on the method of Richards (1991) for obtaining equivalent neutral winds from the height of the F2 peak electron density was used in the model of the ionosphere and plasmasphere. The $O^+ - O$ collision frequencies given by Salah (1993) and the MSIS-86 model with the adjusted N_2 and O_2 densities were used in the IZMIRAN model

Boltzmann distribution with temperature T_n. The calculations showed that the vibrational temperature during the quiet period 16–17 March is less than during the magnetic storm period 18–23 March. During the daytime, T_v is larger than T_n, due to the enhanced thermal excitation of N_2 as a result of high thermal electron temperatures at F2-region altitudes. On 16–22 March the value of the vibrational temperature was not more than 1600 K.

Figure 1 (solid lines) shows NmF2 and hmF2 calculated by using the non-Boltzmann vibrational distribution of N_2, and solid and dotted lines of Fig. 3 give the comparison of the modeled densities using the Boltzmann and non-Boltzmann vibrational distribution of N_2. It can been seen that the Boltzmann-distribution assumption can lead to an increase in the calculated daytime NmF2 of up to a factor of 1.1 and to a decrease in the disturbed nighttime NmF2 by up to a factor of 1.2 in comparison with NmF2 calculated by using the non-Boltzmann vibrational distribution of N_2.

3.4 EUV Flux

Figure 5 shows ratios of the measured NmF2(exp) to the modeled NmF2(th) during the 16–23 March 1990 period for the EUVAC solar flux model (solid line) and the EUV94X solar flux model (dashed line). The modeled densities were obtained using the non-Boltzmann vibrational distribution of N_2. The method of Eqs. A. 18, A.20 based on the Richards (1991) approach for obtaining equivalent neutral winds from the height of the F2 peak electron density and CEDAR standard (Eqs. 3) for the O^+–O frequency (Salah, 1993) were used in the model. The model results were obtained when the recombination rate of the $O^+(^4S)$ ions was multiplied by the factor of 1.5 at all altitudes during the nighttime time-periods of 16–18 March and 19–20 March when the solar zenith angle was more than 90° in the northern hemisphere.

From Eqs. A.1, A.3–6, it follows that during daytime periods the photoionization frequencies $I_1, I_2,$ and I_3 for atomic oxygen give a linear relationship between NmF2 and the solar EUV fluxes. The EUVAC model (Richards et al., 1994a) and the EUV94X model (Tobiska, 1993, 1994) are usually used to calculate the solar EUV fluxes. The ratios of $I_1, I_2,$ and I_3 given by EUV94X to $I_1, I_2,$ and I_3 given by EUVAC are 1.52–1.65, 1.38–1.48, and 1.39–1.49, respectively for 16–23 March. Therefore in Fig. 5 the use of EUV94X increases the modeled NmF2 in comparison with NmF2 calculated using EUVAC.

Our model uses analytical formulae to describe the production of $O^+(^4S), O^+(^2D), O^+(^2P), NO^+, O_2^+,$ and N_2^+ ions by photoelectron impact (Pavlov, 1994). If the optical depth of the atmosphere goes to zero then production frequencies I_{1e}, I_{2e} and I_{3e} of the $O^+(^4S), O^+(^2D),$ and $O^+(^2P)$ ions due to photoelectrons can be calculated from Eq. A.7. We found that in this case $I_{1e}/I_1 = 0.46 - 0.47,$ $I_{2e}/I_2 = 0.63 - 0.64,$ $I_{3e}/I_3 = 0.65 - 0.66$ when the EUVAC model fluxes are used and $I_{1e}/I_1 = 0.29 - 0.30, I_{2e}/I_2 = 0.44, I_{3e}/I_3 = 0.45 -0.46$ when we use EUV94X model fluxes. Therefore the higher photoionization rate using EUV94X compared to EUVAC is partially compensated by the smaller rate of production by photoelectron impact, in agreement with the conclusions of Buonsanto et al. (1995). The resulting effect on the NmF2 is an approximate 10–30% increase in NmF2 using the EUV94X model compared to the EUVAC model, and this effect is largest during the daytime periods.

As seen from Fig. 4, the modeled NmF2 are largest when EUV94X is used. The model results obtained using the EUVAC flux model agree a little better with the observations in comparison with using the EUV94X flux model. If we use the EUVAC model, then in general the Boltzmann vibrational N_2-distribution assumption gives better agreement between measured and modeled NmF2 than the non-Boltzmann vibrational distribution of N_2. To improve this agreement in the ionospheric
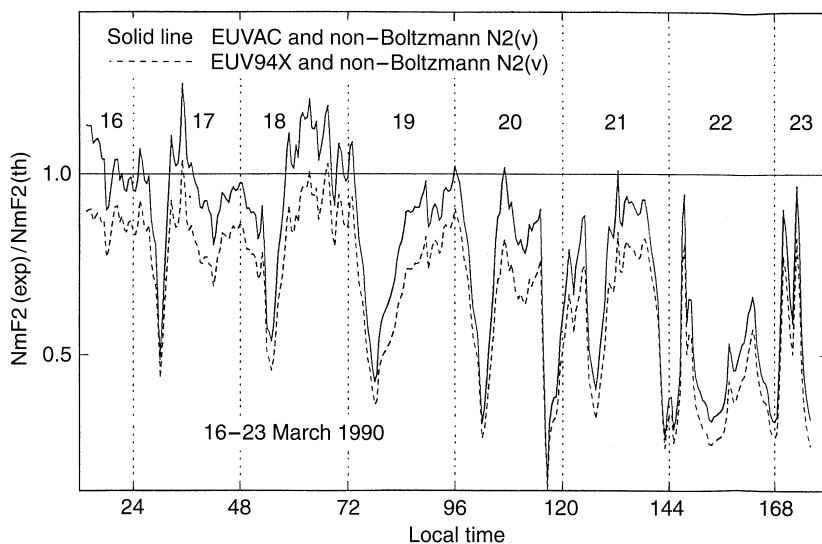

Fig. 5. Ratios of the measured F2 peak densities NmF2(exp) to the modeled F2 peak densities NmF2(th) during the 16–23 March 1990 period for the EUVAC solar flux model (solid line) and the EUV94X solar flux model (dashed line). The modeled NmF2 were obtained using the non-Boltzmann populations of the first five vibrational levels by solving the $N_2(v = 1-5)$ time-dependent continuity equations, the O^+ –O collision frequencies given by Salah (1993), and the MSIS-86 model with adjusted recombination rate of the $O^+(^4S)$ ions

model with EUV94X fluxes, the non-Boltzmann vibrational distribution of N_2 is needed.

3.5 Electron and ion temperatures

Figure 6 shows the diurnal variations of the measured (solid lines) and modeled (dashed and dotted lines) electron and ion temperatures at the F2 peak altitude for the EUVAC solar flux model. The O^+–O frequencies given by Salah (1993) and the method of Eqs. A.18, A.20 based on the Richards (1991) approach for obtaining equivalent neutral winds from the height of the F2 peak electron density and the adjustment of the recombination rate of the $O^+(^4S)$ ions was used in the model of the ionosphere and plasmasphere. The model results were obtained using the non-Boltzmann vibrational N_2 (v) distribution (dashed lines), and when N_2 (v) was not included in the loss rate of the $O^+(^4S)$ ions (dotted line). As can be seen, the effects on T_e of adding N_2 (v) are largest during the day, with increases in T_e accompanying the decreases in NmF2, improving the agreement with observations.
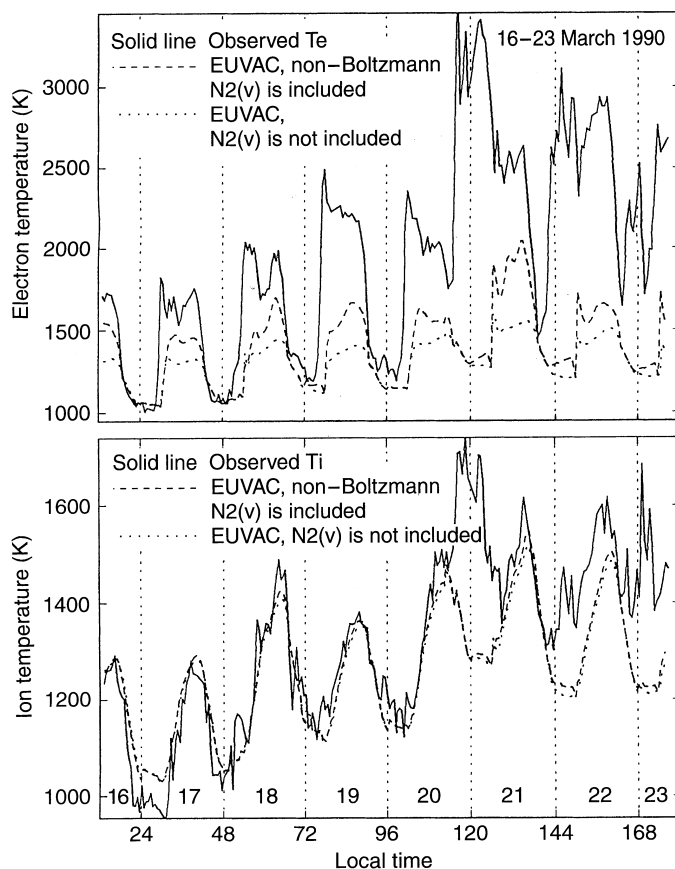

Fig. 6. The measured (*solid lines*) and modeled (*dashed and dotted lines*) electron (*top*) and ion (*bottom*) temperatures at the F2 peak altitude on 16–23 March 1990 for the EUVAC solar flux model. The *dashed lines* show results when the non-Boltzmann populations of the first five vibrational levels of $N_2(v)$ are included in the model, and the *dotted lines* are ones without the effects of vibrationally excited N_2 on the loss rate of the $O^+(^4S)$ ions

During the period 16–18 March the agreement between the measured and modeled temperatures is excellent except during the short time-periods around 5.00–7.00 LT for the electron temperature. These measured short-duration electron-temperature enhancements near these sunrise regions were not described by the model. On 19 March the agreement is satisfactory for the electron temperature and is good for the ion temperature. The modeled electron temperatures are generally lower than the measured electron temperatures after the 20 March storm. The electron-ion cooling rate is proportional to the square of the electron density, and therefore if the electron density is too large, then the electron temperature is too small, as is apparent during the day for 19 and 22 March. When N_2 (v) is not included in the loss rate of the $O^+(^4S)$ ions, the agreement between the model and the data worsens. From our calculations it follows that the use of the EUVAC flux model gives better agreement between measured and modeled electron temperatures than the EUV94X flux model, because the modeled electron temperatures are higher as a consequence of the modeled NmF2 being lower (see Fig. 5). The effects of the flux model and N_2 (v) on the calculation of T_i are not very large.

3.6 FLIP and IZMIRAN models- data comparisons

Richards *et al.* (1994b) compared observed values of NmF2, hmF2, T_e, and T_i at Millstone Hill with FLIP model results for the March 1990 storm. Unlike the results shown in Fig. 1, calculations with the FLIP model without including N_2 (v) gave good agreement with the data on 18–20 March. However, the inclusion of N_2 (v) improved the agreement with the data during the disturbed period 21–23 March.

The FLIP and the IZMIRAN models are very similar models of the thermal plasma in the ionosphere and plasmasphere. Both solve the coupled time-dependent energy, momentum, and continuity equations for major ions and electrons, and photoelectron transport equations from the base altitude in both hemisphere, along a field line to the same base altitude in the other hemisphere.

Both the FLIP model and the IZMIRAN model use the theoretical interpretation of the flow-drift tube measurements of the recombination-rate coefficient of $O^+(^4S)$ ions with $N_2(v = 0)$ (Albritton *et al.*, 1977) and formulas for the dependence of this rate coefficient of the effective temperature given by St.-Maurice and Torr (1978). For vibrationally excited N_2, the FLIP model uses only the recombination-rate coefficients of $O^+(^4S)$ ions with $N_2(v > 0)$ measured by Schmeltekopf *et al.* (1968) only for $T_n = T_i = 300$ K. The IZMIRAN model uses theoretical formulas given by Pavlov (1988) based on the measurements of Schmeltekopf *et al.* (1968). The temperature dependence given by Van Zandt and O'Malley (1973) determines the dependence of these rate coefficients on the effective temperature in the IZMIRAN model. In the FLIP model $K_1(T)/K_0(T) = 1, K_2(T)/$

$K_0(T) = 38$, $K_3(T)/K_0(T) = 85$, $K_4(T)/K_0(T) = 220$, $K_5(T)/K_0(T) = 270$ where T is the effective temperature.

The heated drift tube measurements of the recombination-rate coefficient of $O^+(^4S)$ ions with O_2, γ, given by Chen et al., (1978) are systematically lower than the flow-drift tube measurements, γ_E, of this rate coefficient Albritton et al., 1977. In an attempt to reconcile the two sets of measurements, the IZMIRAN model (Pavlov, 1993) uses $\gamma = \gamma_E \exp(-8.53.10^{-4} T_n + 0.315)$ with the approximation for γ_E given by St.-Maurice and Torr (1978). Torr et al. (1990) normalized the drift tube date of Albritton et al. (1977) on the results of Chen et al. (1978) at 700 K and obtained $\gamma = 2.1 \cdot 10^{-11}$ $(T_n + 2T_i/3 \times 300)^{-0.763} cm^3 s^{-1}$ which is used in the FLIP model.

The quenching of $O^+(^2D)$ by atomic oxygen is assumed to be $10^{-10} cm^3 s^{-1}$ (Oppenheimer et al., 1976; Fox and Dalgarno, 1985) in the IZMIRAN model and $5 \cdot 10^{-12}$ (Abdou et al., 1984) in the FLIP model. These rate coefficients were obtained from agreement between the measured and model densities of N_2^+ and the different points of view were discussed by Torr and Torr (1982), Abdou et al., (1984), Ferguson (1984), and Fox and Dalgarno (1985). This discussion illustrates that laboratory measurements of this rate coefficient are highly desirable.

The FLIP model solves the two-stream photoelectron Liouville equations to calculate the photoelectron fluxes, and these fluxes are used to find the heating rate of the electron gas by photoelectrons and the rate of ionization by secondary photoelectrons. In the IZMIRAN model, electron heating due to photoelectrons is provided by a solution of the Boltzmann equation for photoelectron flux using the method of Krinberg and Tashchilin (1984). The IZMIRAN model uses the approximative approach of Pavlov (1994) to calculate the rate of ionization by secondary photoelectrons.

These differences between the FLIP model and the IZMIRAN model give the differences in the model results for the March 1990 magnetic storm.

4 Undisturbed period and storms of 6–12 April 1990

The undisturbed conditions of 6–8 April 1990 and the 9–12 April 1990 magnetic storms were periods of moderate solar activity, when the 10.7 solar flux varied between 146 and 169 and A_p between 6 and 124. During the April 1990 period, two geomagnetic storms took place with sudden commencement times near 0842 UT on 9 April and 0325 UT on 12 April. The measured electron densities and temperatures and ion temperatures used in this paper were taken by the incoherent-scatter radar at Millstone Hill, Massachusetts (Buonsanto et al., 1992a).

Figure 7 is a plot of the measured hmF2 and NmF2 for the period 6–12 April 1990 and the model results which will be discussed later. The model results have been obtained from the mathematical model with the O^+–O collision frequencies given by Salah (1993), the original MSIS-86 model, and the approach of Eqs. A.18,
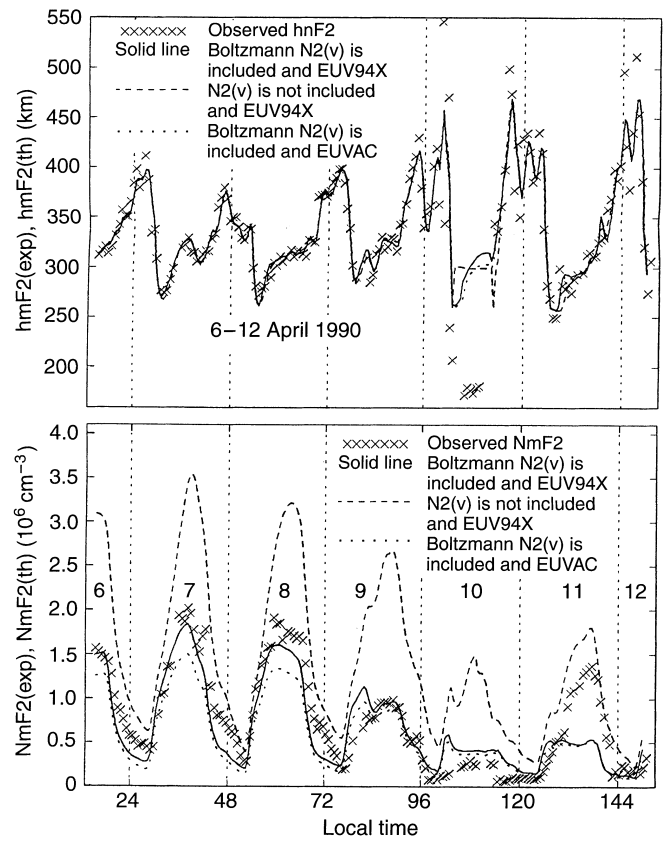

Fig. 7. Observed (crosses) and calculated F2 peak parameters above Millstone Hill for the magnetically quiet and disturbed period 6–12 April 1990 for the EUV94X solar flux model (solid and dashed lines) and the EUVAC solar flux model (dotted lines). The solid and dotted lines are hmF2 and NmF2 from the IZMIRAN model when the Boltzmann populations of the first five vibrational levels of N_2 (v) are included in the calculated $O^+(^4S)$ recombination rate, and dashed are hmF2 and NmF2 when N_2 (v) is not included in the calculations

A.20 based on the improved algorithm given by Richards (1991).

Unlike the March period, there are only negative phases in the measured NmF2 compared to the undisturbed period of 6–7 April. The most notable feature of this period is the disappearance of the F2 peak on 10 April, when the peak height of the electron-density maximum dropped to 180 km.

In modeling the April magnetic storm we also used the theoretical formulae of the 1–3 for the O^+–O collision freqency. Like the results of March in Fig. 2, the Salah (1993) collision frequency resulted in NmF2 which were approximately 5–17% larger than those calculated using the Banks (1966) formulae. Again, the Salah (1993) formulae gave the best agreement between measured and modeled NmF2.

Figure 7 shows that similar to the March period, the EUV94X model (solid lines) produced the largest electron densities, increasing NmF2 by about 10–40% compared to the EUVAC model (dotted lines). Unlike the March period, for the period 6–9 April 1990 the EUV94X model results agree better with the observations in comparison to using the EUVAC model.

Like the 17–18 March and 19–20 March period, on 6–9 April the nighttime measured densities were a factor of up to 1.5–2 larger than the model densities. There may be an unidentified physical or chemical process that has not been included in the IZMIRAN model. It is possible that this nighttime discrepancy between measured and modeled NmF2 is caused by inaccuracies in key inputs, such as the composition and temperature of the neutral atmosphere, and the recombination-rate coefficients of $O^+(^4S)$ ions with $N_2(j = 0-5)$ and O_2. From our calculations it follows that in order to reproduce the observed nighttime NmF2 on 6–10 April the recombination rate of $O^+(^4S)$ ions needs to decrease by a factor of 1.5 at all altitudes during the nighttime 6–7 April, 7–8 April, and 9–10 April periods when the solar zenith angle was more than $90°$ in the northern hemisphere.

The method of Eqs. A.18, A.20 reproduces well the measured hmF2 during the quiet and disturbed periods on 6–9 April except for the unusually large fluctuations in peak height such as occurred on 10 April. The method of deriving the equivalent neutral wind from the observed hmF2 does not work if the peak layer is in the F1 region. Also, the equivalent winds will be contaminated with any large electric fields such as were present at the beginning and end of the disappearance of the F2 layer (Buonsanto *et al.*, 1992a; see also Fig. 10. discussed later). On 9–11 April the theoretical NmF2 sometimes describes the experimental data well, but often the calculated NmF2 differs greatly from the measured NmF2. Some reasons for these disagreements are that we do not take into account the effect of electric fields on the ionosphere and the MSIS model does not predict neutral densities and temperature accurately during some geomagnetic storms. The effects of the electric fields on the electron density and the ion temperature are presented in the next section.

Figure 7 (bottom panel) shows that the modeled peak densities without effects of vibrationally excited $N_2(v)$ (dashed line) are much larger than the modeled peak densities with $N_2(v)$ (solid line). Both the daytime and nighttime measured densities are not reproduced by the model without $N_2(v)$. On 6–12 April this effect of $N_2(v)$ on NmF2 is up to a factor of about 3.5 reduction, similar to the case for the March period. In both March and April magnetic storms, the effect of vibrationally excited N_2 on N_e and T_e is most pronounced during the daytime.

In modeling the April magnetic storm we also calculated deviations from the Boltzmann distribution of $N_2(v)$. Like the results of March in Fig. 4, the real distribution is highly non-Boltzmann at the vibrational levels $j > 2$ and the deviations from the Boltzmann distribution are not significant at the first and second vibrational levels of N_2. Nevertheless, the values of the relative deviations $n_3/n_{3B} < 3.2$ and $n_4/n_{4B} < 17$. The deviations on third and fourth vibrational levels of N_2 have their maximum values during the period 6.30–7.30 LT. The April variations of the calculated vibrational temperature are very similar to that for Millstone Hill on March 1990. Similar to the March case, the

Boltzmann-distribution assumption can lead to a 10–20% increase in the calculated NmF2 in comparison with NmF2 calculated using the non-Boltzmann vibrational distribution of N_2.

The diurnal variations of the measured (solid lines) and modeled (dashed and dotted lines) electron and ion temperatures at the F2 peak altitude are shown in Fig. 8. The O^+-O frequencies given by Salah (1993) and the method of Eqs. A.18, A.20 for obtaining equivalent neutral winds from the height of the F2 peak electron density were used in the model of the ionosphere and plasmasphere. The model results were obtained using the EUV94 solar flux model with the Boltzmann vibrational N_2 distribution (dashed lines) and when $N_2(v)$ is not included in the loss rate of the $O^+(^4S)$ ions (dotted line). The modeled ion temperatures with the Boltzmann vibrational N_2 distribution are about the same as when $N_2(v)$ is not included.

During the quiet and disturbed period 6–9 April the agreement between the measured and modeled temperatures is excellent except for the time period 4.30–6.00 LT for the electron temperature. This measured, short-duration electron-temperature enhancement near the sunrise region was not described by the model. Electric
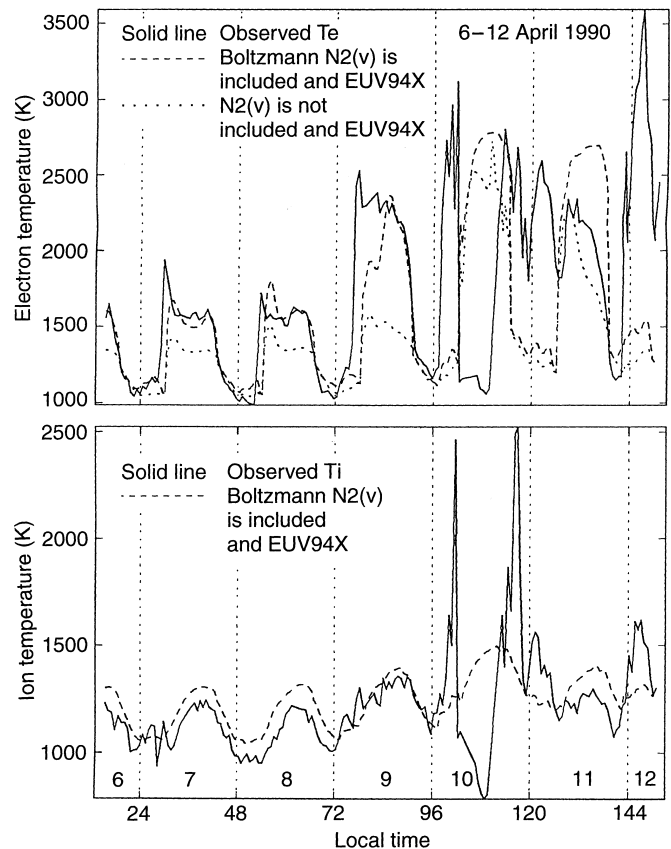

Fig. 8. The measured (*solid lines*) and modeled (*dashed and dotted lines*) electron (*top*) and ion (*bottom*) temperatures at the F2 peak altitude 6–12 April 1990 for the EUV94X solar flux model. The *dashed lines* show results when the Boltzmann populations of the first five vibrational levels of $N_2(v)$ are included in the model and the *dotted line* is one without effects of vibrationally excited N_2 on the loss rate of the $O^+(^4S)$ ions

fields larger than 30 mV/m^{-1} were present around 6 and 18 LT on 10 April and also during the first part of 12 April when the modeled ion and electron temperatures are significantly smaller than the observations. The large model ion and electron temperatures, during the middle of the day on 10 April reflect the fact that they are F2-region temperatures, while the observations are in the F1 region with the disappearance of the F2 electron density peak. When $N_2(v)$ is not included in the loss rate of the $O^+(^4S)$ ions, the agreement between the model and the data worsens in comparison with its inclusion, with the exception of the daytime period on 10 April when the measured peak electron density was in the F1 region.

5 Effect of measured electric fields and meridional neutral winds on electron density

The short-lived electric fields produce significant effects on N_e and the ion temperature, T_i (Schunk et al., 1975; Raitt et al., 1976). These changes in the electron density and ion temperature are the reason for the electron-temperature disturbances. These electric fields were stronger during the April 1990 storm than during the March 1990 storm at Millstone Hill (Buonsanto et al., 1992a).

The values of perpendicular electric fields $E_\perp$ (with respect to $\boldsymbol{B}$) and meridional neutral winds were measured during the March and April 1990 magnetic storms (Buonsanto et al., 1992a). Using these measured neutral winds we can calculate the wind-induced plasma drift velocity in the direction along a magnetic field line as $W_d = U_\theta \cos I$, where I is the magnetic field dip angle, U_θ is the component of thermospheric wind in spherical polar coordinates, and θ is the geomagnetic colatitude. After that we can use these W_d as input data in the model of the thermal plasma in the ionosphere and plasmasphere.

We use two important changes of the IZMIRAN model given by Pavlov (1996) to take into account the effect of $E_\perp$ on N_c and T_i. To model the effect of $E_\perp$ on T_i we added the local ion-heating rate due to perpendicular electric fields, $Q_{i\perp} \sim E_\perp^2$, given by Schunk et al. (1975) in the ion-energy equation of the IZMIRAN model. The rate coefficients of the important ionospheric processes such as the reaction of $O^+(^4S)$ with N_2 and O_2 depend on the effective temperature which is a function of the ion temperature, the neutral temperature, and the plasma drift velocity (Albritton et al., 1977; Viehland and Mason, 1977; St.-Maurice and Torr, 1978; Pavlov, 1988). The plasma drift velocity is resolved into components parallel and perpendicular to the geomagnetic field, $\boldsymbol{B}$, with the perpendicular component

$$V_\perp = (\boldsymbol{E} \times \boldsymbol{B})/\boldsymbol{B}^2, \qquad (8)$$

where $\boldsymbol{E}$ is the electric field.
This dependence of the recombination rate of $O^+(^4S)$ ions on $E_\perp$ gives the effect of $E_\perp$ on N_e.

In Figs. 9–10 we present the measured hmF2 and NmF2, the measured $E_\perp$ at the hmF2 altitude (Buon-

santo et al., 1992a), and the model results during the 16–23 March and 6–8 April 1990 periods. The dashed lines show the results when we used in the model without $E_\perp$ the algorithm (Eqs. A.1, A.20) for obtaining equivalent neutral winds from the height of the F2 peak electron density, whereas the dotted lines were obtained when the measured $E_\perp$ and meridional neutral winds were used.

From Figs. 9 and 10, the observed hmF2 s are generally lower during the day and the night, except for the very brief nighttime periods 17–22 March and 10–12 April compared to the hmF2 s derived using measured $E_\perp$ and the meridional neutral wind. Figures 9 and 10 show that the effect of using $E_\perp$ and the meridional neutral wind instead of the measured hmF2 results in higher values of NmF2 both day and night, and in higher values of hmF2 during the most part of the 16–23 March and 6–8 April periods. Since using the measured hmF2 often results in nighttime NmF2 values which are too low compared to observations, this often means that using the $E_\perp$ and meridional neutral wind results in better nighttime agreement during the March storm. However, the values during the day are usually higher than the observations and the results using hmF2 observations. Since using the data does not always give theoretical values that agree better with other observations such as NmF2, there are other sources of uncertainty, such as the model input parameters, physical processes, and errors in the measurements.

For the April storm Fig.10 also gives the measured T_i at the hmF2 altitude (Buonsanto et al., 1992a) and the calculated T_i. As can be seen, the effects using $E_\perp$ and the meridional neutral wind instead of the measured hmF2 on T_i are largest on 10 April with increases in T_i up to about 230 K, making worse the agreement with observations during the middle of the day on 10 April because the modeled T_i are F2-region ion temperatures, while the measured T_i are the F1-region ion temperatures. For the March storm these increases in T_i are less than 50 K.

Extremely low NmF2 and hmF2 (rather, it was the F1 peak) were observed between 9.30 and 14.30 LT on 10 April (Buonsanto et al., 1992a). Our calculations indicate that the electron density, decreases if the electric-field strength increases due to the increased rates of the reactions $O^+(^4S)$ with N_2 and O_2 relative to the zero electric field result while the NO^+ and O_2^+ densities are increased. For $E_\perp \sim 90\text{–}100$ mV m^{-1}, the decrease in $O^+(^4S)$ ion density is sufficient to cause the density of molecular ions to be greater than the $O^+(^4S)$ ion density. As a result the usual F2 region peak created by $O^+(^4S)$ ions vanishes, the new F2 region peak (rather it is the F1 peak) due to molecular ions results, and the extremely low observed NmF2 and hmF2 can be explained. However, $E_\perp \sim 90 - 100\,\mathrm{m\,V\,m}^{-1}$ were not observed between 9.30 and 14.30 LT on 10 April (Buonsanto et al., 1992a) and therefore the model was unable to account for the observed NmF2 and hmF2.

Data show a decrease in the electric fields around midday, but the larger electric fields in the morning may have produced some longer-lasting changes in the neutral temperature and the neutral composition, which
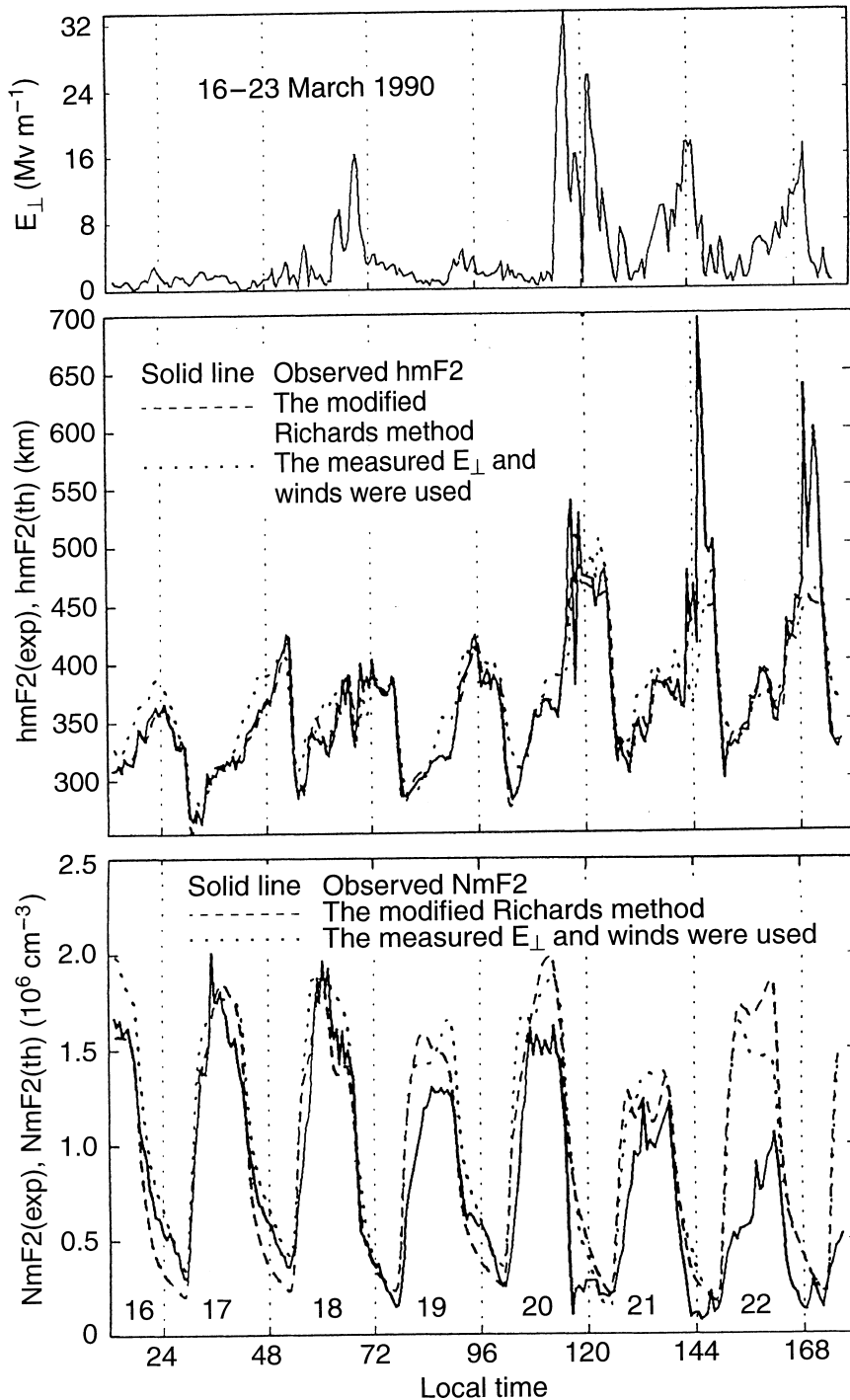
Fig. 9. The measured $E_\perp$ at the hmF2 altitude (*top panel*), the measured and modeled hmF2 (*middle panel*), and the measured and modeled NmF2 (*bottom panel*) during the 16–23 March 1990 period for the EUVAC solar flux model. The solid lines are the Millstone Hill data (Buonsanto *et al.*, 1992a). The *dotted lines* show the results when we use no $E_\perp$ in the model and the approach based on the method of Richards (1991) for obtaining equivalent neutral winds from the height of the F2 peak electron density, whereas the *dashed lines* were obtained when the measured $E_\perp$ and meridional neutral winds were used. All the model results have been obtained from the IZMIRAN model with the Boltzmann populations of the first five vibrational levels of $N_2(v)$, the $O^+ - O$ frequencies given by Salah (1993) and the original recombination rate of $O^+(^4S)$ ions

are not included in the MSIS-86 model, and as a result the modeled N_e may be larger than the data near midday on 10 April. Another explanation of the disagreement between the modeled N_e and the data on 10 April is that this plasma depletion in the flux tube with extremely low NmF2 and hmF2 can be created in the mid-latitude trough by horizontal plasma convection. To model this transfer of plasma, caused by some plasmaspheric electric field (usually of magnetospheric origin), consideration of the perpendicular divergence contribution in the ion equations of continuity arising from

horizontal plasma gradients is needed, and a model of this electric field is required or must be created. We intend to solve these tasks in future studies by the development of the IZMIRAN model.

6 Forecast of NmF2 and hmF2 during magnetic storms

In modeling electron densities it is important to reproduce hmF2 which is primarily influenced by the neutral wind. Richards (1991) developed an algorithm

that ensures a close reproduction of the observed hmF2 by a time-dependent model. Ideally, the observed hmF2 should be available for several hours before the time of the comparison, but very often only a limited set of hmF2 measurements is available or we have not got the observed hmF2, To overcome this problem, we can use Eqs. A.21–23 to calculate equivalent plasma drift velocities during geomagnetic storms.

Figures 11 and 12 represents the modeled hmF2 and NmF2 (the solid lines) obtained when this approach was used. For both the March and April magnetic storms the errors in the prediction of the modeled NmF2 are about the same as when we use the measured hmF2 and the Richards (1991) method with our modification A.18, A.20 to calculate an equivalent plasma drift velocity. In our approach (Eqs. A.21–A.23), the measured and modeled daytime hmF2 agreed better than the nighttime hmF2. The disagreement between the measured and calculated hmF2 is not more than 14, 36, 63, 41, 144, 64, 264, and 184 km on the nights of March 16–23, and not more than 9, 19, 40, 27, 19, 56, 28, and 36 km on days of 16–23. On the nights of 8–12 April the disagreement between the measured and calculated hmF2 is not more than 22, 58, 204, 43, and 78 km, and not more than 15, 50, 121, and 75 km on days of 8–11.
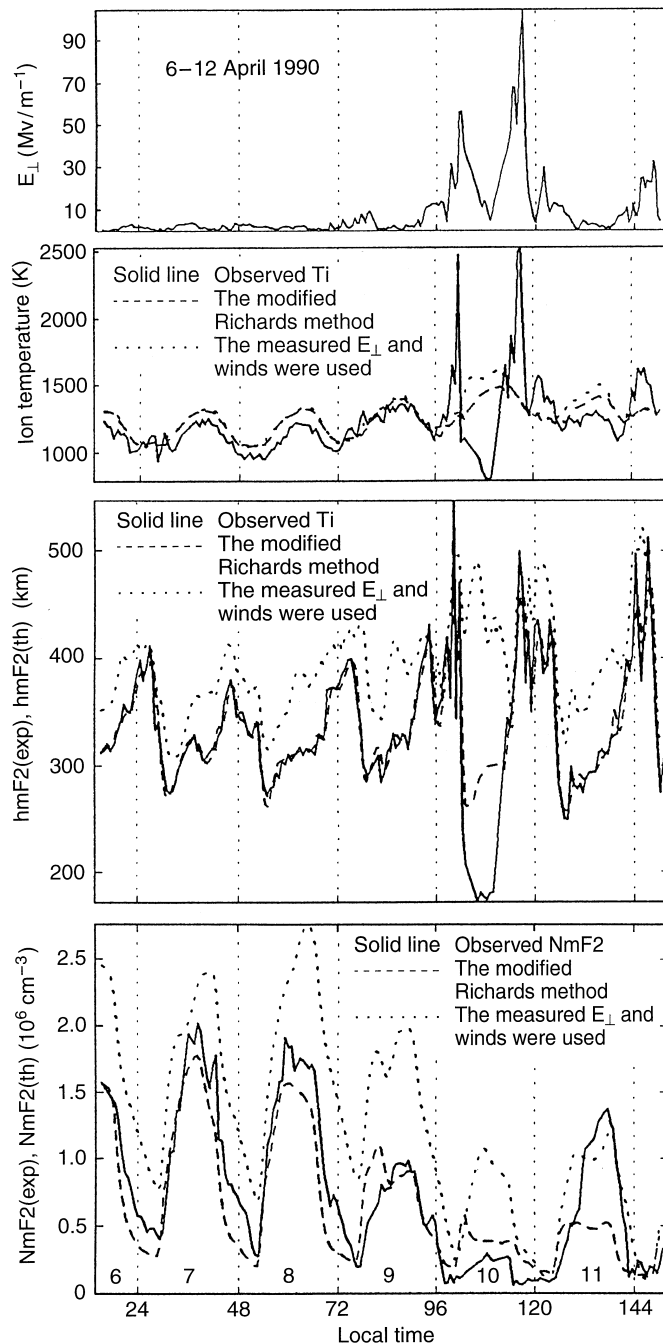

Fig. 10. The measured $E_\perp$ at the hmF2 altitude (*top panel*), the measured and modeled T_i hmF2 (*two middle panels*), and the measured and modeled NmF2 (*bottom panel*) during the 6–12 April 1990 period for the EUV94X solar flux model. The *solid lines* are the Millstone Hill data (Buonsanto *et al.*, 1992a). The *dotted lines* show the results when we use in the model no $E_\perp$ and the approach based on the method of Richards (1991) for obtaining equivalent neutral winds from the height of the F2 peak electron density, whereas the *dashed lines* were obtained when the measured $E_\perp$ and meridional neutral winds were used. All the model results have been obtained from the IZMIRAN model with the Boltzmann populations of the first five vibrational levels of $N_2(v)$, the $O^+ - O$ frequencies given by Salah (1993), and the original recombination rate of $O^+(^4S)$ ions
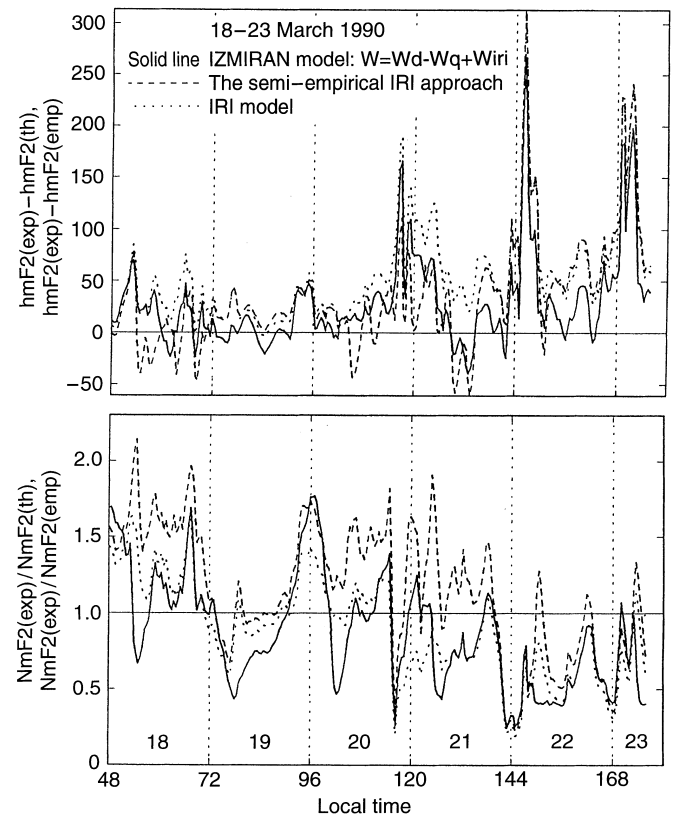

Fig. 11. Comparison of measured NmF2(exp) and hmF2(exp) with peak densities and heights NmF2(th) and hmF2(th) given by the IZMIRAN model with algorithm Eq. A.23 (*the solid lines*) and NmF2(emp) and hmF2(emp) given by the IRI-90 model (*the dotted lines*) and by the semiempirical IRI approach described by Kishcha (1995) (*the dashed lines*) for the disturbed period of 18–23 March 1990. The Boltzmann vibrational distribution of $N_2(v)$, and the original recombination rate of $O^+(^4S)$ ions are implied in the IZMIRAN model
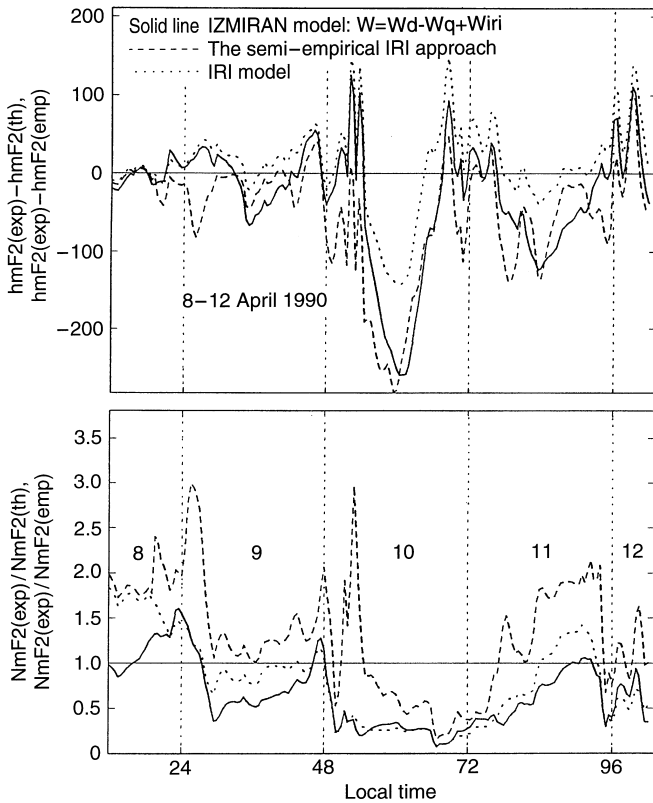
Fig. 12. Comparison of measured densities and heights with peak densities and heights given by the IZMIRAN model, the IRI-90 model, and the semiempirical IRI approach described by Kishcha (1995) for the period of 6–12 April 1990. The curves are the same as in Fig. 11

By using the algorithm (Eqs. A.21–A.23), we can forecast the values of NmF2 and hmF2 during magnetic storms. Such predictions of NmF2 and hmF2 are also possible to carry out using the semiempirical IRI approach described by Kishcha (1995) (a discussion of this approach is in Appendix A). In addition to storm effects, the semiempirical IRI approach takes into account substorm effects in NmF2 and hmF2.

The dotted and dashed lines in Figs. 11 and 12 show results when the modeled F2 peak densities and heights are given by IRI-90 (Bilitza, 1990) and the semiempirical IRI approach described by Kishcha (1995) (both storms and substorms inputs) were used. We can see that sometimes the theoretical results and the semiempirical IRI approach describe the experimental data well, but often they differ greatly from the measured NmF2 and hmF2. To establish how good or bad a forecast can be it is necessary to define a quantitative measure of its success. For a large number (M) of forecasts of NmF2

and hmF2 during magnetic storms, we can compute root-mean-square errors as

$$\varepsilon_1 = \left\{ \sum_{s=1}^{M} [\text{hmF2}_s(\text{exp}) - \text{hmF2}_s(f)]^2 / M \right\}^{1/2}, \quad (9)$$

$$\varepsilon_2 = \left\{ \sum_{s=1}^{M} [\text{NmF2}_s(\text{exp}) - \text{NmF2}_s(f)]^2 / M \right\}^{1/2}, \quad (10)$$

where hmF2_S (exp) and NmF2_S (exp) are the measured hmF2 and NmF2 and $\text{hmF2}_S(f)$ and NmF2_S (f) are forecasts of NmF2 and hmF2 given by IRI-90, the semi empirical IRI approach and the IZMIRAN model.

Table 1 gives the calculated ε_1 and ε_2 for the 18–23 March and 8–12 April storm periods. We can see that the use of the semiempirical IRI approach gives a slightly better agreement between measured and modeled NmF2 than the IZMIRAN model, and the semi empirical IRI approach gives the worst forecast of hmF2. The best agreement between the measured and modeled hmF2 is the IZMIRAN model for the March storm and the IRI-90 model for the April storm. In general, our results do not confirm very optimistic conclusions given by Kishcha (1995): "the IRI model can significantly be improved under disturbed conditions up to the factor 2 on the average with the proposed updating technique". There is no reason to assert that conditions from Eqs. A.9, A.10, A.13 (see Appendix A) that form the basis for derivation of the analytical equations used by Kishcha (1995) are valid during all storms, but during some storms Eqs. A.14, A.15 may be valid with some errors.

In modeling the March and April magnetic storms we had the measured hmF2 and we used the method developed by Richards (1991) with our modification Eqs. (A.18, A.20) to calculate an equivalent plasma drift velocity. If we use the resulting NmF2 instead of NmF2(f) in Eq. 10 then $\varepsilon_2 = 1.8 \cdot 10^5 \text{cm}^{-3}$ $\varepsilon_2 = 3.0$ 10^5cm^{-3} for the 18–23 March and 8–12 April periods. These inaccuracies in the modeled NmF2 are less than those given by the IZMIRAN model using the algorithm Eqs. A.21–A.23) for the April storm. However, for the 18–23 March period, the root-mean-square error of NmF2 given by the IZMIRAN model is less if the algorithm (Eqs. A. 21–A.23) is used.

7 Conclusions

A comparison of the Millstone Hill ionospheric-storm-time measurements of the electron density and temperature with the model results is presented for the

| | 18–23 March | | 8–12 April | |
	ε_1 (km)	ε_2 (10^5 cm^{-3})	ε_1 (km)	ε_2 (10^5 cm^{-3})
IRI-90	73	1.7	55	3.9
Kishcha (1995)	66	1.3	89	3.3
The IZMIRAN model	52	1.5	80	3.8

Table 1. Forecasting root-mean-square errors of hmF2 and NmF2

magnetically quiet and disturbed periods on 16–23 March and 6–12 April. The CEDAR standard (Eq. 3) for the ion-neutral O^+–O collision frequency for momentum transfer presented by Salah (1993), which is larger than other commonly accepted frequencies, gives the best agreement between measured and modeled NmF2. The recombination rate of $O^+(^4S)$ ions was decreased by a factor of 1.5 at all altitudes during the nighttime periods 17–18 March 19–20, March 6–7, April 7–8 April and 9–10 April in order better to increase the NmF2 at night to match observations.

We often have not obtained the observed hmF2 and cannot use the method based on the Richards (1991) approach. In this case the IRI hmF2 can be used to calculate an equivalent plasma drift velocity for undisturbed conditions by using the modified Richards method. After that we can calculate the wind-induced plasma drift velocity for undisturbed and disturbed conditions in the usual way, without using the IRI hmF2, by solving two momentum equations for the horizontal components of thermospheric wind. Finally, we obtain the plasma drift velocity in the ion continuity equations $W = W_d - W_d - W_q + W_{IRI}$. On 8–12 April the inaccuracy in the modeled NmF2 ($3.8 \cdot 10^5\,\mathrm{cm}^{-3}$) is about the same as when we use the measured hmF2 and the modified Richards (1991) method ($3.0 \cdot 10^5\,\mathrm{cm}^{-3}$). For the 18–23 March 1990 period, the root-mean-square errors of NmF2 given by the IZMIRAN model with and without using the measured hmF2 are $1.8 \cdot 10^5\,\mathrm{cm}^{-3}$ and $1.5 \cdot 10^5\,\mathrm{cm}^{-3}$, and the forecast of NmF2 is better if the algorithm of Eqs. A.21–A.23 is used.

Inclusion of vibrationally excited N_2 brings the model and data into better agreement. For both March and April the effect of vibrationally excited N_2 on N_e and T_e is most pronounced during the daytime, with factors of up to 4 and 3.5 reduction in the daytime peak density for March and April, respectively, due to the inclusion of vibrationally excited N_2.

The derivations from the Boltzmann distribution for the first five vibrational levels of N_2 were calculated. The present study suggests that the calculated distribution is highly non-Boltzmann at the vibrational levels $j > 2$, and the deviations from the Boltzmann distribution are not significant at the first and second vibrational levels of N_2. It was found that the Boltzmann-distribution assumption can lead to the 10–20% increase in the calculated NmF2 in comparison with NmF2 calculated using the non-Boltzmann vibrational distribution of N_2. The calculations also showed that the vibrational temperature during the quite periods is less then during, the magnetic-storm periods. During the daytime the high vibrational temperature stems from the enhanced thermal excitation of N_2 as a result of high thermal electron temperatures at F2-region altitudes, while the decrease in the vibrational temperature compared to the regular temperature is due to the decreases in the electron density and the neutral temperature.

During the March storm at solar maximum the model results obtained by using the EUVAC flux model agree a little better with the observations in comparison with those using the EUV94 flux model. If we use

EUVAC model, then in general the Boltzmann vibrational N_2-distribution assumption gives better agreement between measured and modeled NmF2 than the non-Boltzmann vibrational distribution of N_2. To improve this agreement in the ionospheric model with EUV94X fluxes it is necessary to use a non-Boltzmann vibrational distribution of N_2 which is more correct. For the April storm period of moderate solar activity the EUV94X model results agree better with the observations in comparison to using the EUVAC model. The resulting effect on the NmF2 is an approximate 10–40% increase in NmF2 using the EUVAC model. The resulting effect on the NmF2 is an approximate 10–40% increase in NmF2 using the EUV94X model compared to the EUVAC model, and this effect is most pronounced during the daytime.

The preceding results indicate that the extremely low NmF2 and hmF2 between 9.30 and 14.30 LT on 10 April cannot be explained by the effects of the measured electric fields and neutral winds on the ionosphere in the frame of our one-dimensional time-dependent theoretical model. We believe that this plasma depletion in the flux tube with extremely low NmF2 and hmF2 is created in the midlatitude ionospheric trough and this flux tube is transferred by horizontal plasma convection. In general, the use of the measured $E_\perp$ and meridional neutral winds as input model parameters does not improve the agreement between the data and the theoretical results giving higher NmF2. This means that there are other sources of uncertainty in the model, such as uncertainties of model input data and physical processes and errors in the measured $E_\perp$ and meridional neutral winds.

The NmF2 and hmF2 calculated by using the IZMIRAN model with algorithm of Eqs. A.21–A.23, or by using the semiempirical IRI approach given by Kishcha (1995), sometimes describe the experimental data well, but often differ greatly from the measured NmF2 and hmF2. In general, the use of the semiempirical IRI approach gives a slightly better agreement between measured and modeled NmF2 than the IZMIRAN model, and the semiempirical IRI approach gives the worst forecast of hmF2. The agreement between the measured and modeled hmF2 is best when the IZMIRAN model was used during the March and or April storms when the IRI-90 model was used to calculate NmF2.

Appendix A

The IZMIRAN model gives the numerical solution of continuity, energy, and momentum equations, but from this very complicated model it is difficult to find reasons for agreement or disagreement between measured NmF2 and hmF2 and modeled NmF2 and hmF2. For the physical interpretation of our modeled results (but not for calculations of NmF2 and hmF2) we use Eqs. 4 and 5 for nighttime and equations for daytime NmF2 and hmF2 obtained here.

In order to find the analytical solution of the steady-state continuity equation for $O^+(^4S)$ ions [$O^+(^2D)$ and $O^+(^2P)$ ions are not considered] during quiet days, Badin and Deminov (1982) and Badin (1989) assumed that the optical depth of the atmosphere goes

to zero, the drift velocity of the plasma in the vertical direction $W \approx$ const, $T_i \approx$ const, $T_n \approx$ const, $T_e \approx$ const and the effects of N_2^* on the electron density tend to zero. Pavlov (1987) took into consideration the effects of N_2^* on the $O^+(^4S)$ ion density and simplified the NmF2 and hmF2 given by Badin and Deminov (1982) by assuming that $[O]^2/[N_2] \approx$ const and $T_v \approx$ const. If we take into account the $O^+(^2D)$ and $O^+(^2P)$ ions and a production of the $O^+(^4S), O^+(^2D)$, and $O^+(^2P)$ ions due to photoelectrons then

$$\text{NmF2}(\text{cm}^{-3}) \approx I v_{in}^{1/3} \, [O] \, (T_n/L^2)^{1/3} \, \exp(Vf_1), \tag{A.1}$$

$$\text{hmF2}(\text{km}) \approx h_0 + 1.92 \cdot 10^{-2} \, T_n \, (\ln f_0 + f_2 + f_3 V), \tag{A.2}$$

where $h_0 = 300$km, $f_1 = 0.092 + 0.424y$, $f_2 = 6.273y - 6.717$, $f_3 = 1.055y + 0.481$, $y = T_n/(T_i + T_e)$, $y \geq 0.2$, $V = 8.7 \cdot 10^{-4} W v_{in}^{2/3} \, (T_n L)^{-1/3}$, $f_0 = 2.15 \, T_n L \, v_{in}$, v_{in} is momentum transfer collision frequency of $O^+ - O$, L is determined by Eq. 5, the units of $[O]$ are cm^{-3} and the units of W are cm s^{-1}; and Eqs. A.1-A.2 are valid if $|V_{f_1}| < 1$.

The ionization frequency, I, gives a linear relationship between NmF2 and the solar EUV fluxes as follows

$$I = I_1 + I_{le} + [O^+(^2D)] K_1 + [O^+(^2P)]$$
$$\{K_2[O] + K_3[N_2] + K_4\} \, [O], \tag{A.3}$$

where

$$[O^+(^2P)] = (I_2 + I_{2e})[O]/\{K_4 + K_5 + K_2[O] + K_3[N_2]\}, \tag{A.4}$$

$$[O^+(^2D)] = \{(I_3 + I_{3e})[O] + K_5[O^+(^2P)]\}/$$
$$\{K_6[N_2] + K_7[O_2] + K_1[O]\}, \tag{A.5}$$

photoionization production frequencies of the $O^+(^4S), O^+(^2D)$, and $O^+(^2P)$ ions

$$I_1 = \sum_\lambda F(\lambda)\sigma_1(\lambda), \quad I_2 = (\lambda) \sum_\lambda F\sigma_2(\lambda),$$
$$I_3 = \sum_\lambda F(\lambda)\sigma_3(\lambda), \tag{A.6}$$

production frequencies of the $O^+(^4S)$, $O^+(^2D)$, and $O^+(^2P)$ ions due to photoelectrons are calculated by using the approximation approach given by Krinberg (1978) with the correction factor given by Pavlov (1994)

$$I_{le} = \sum_{\lambda=0}^{A} F(\lambda)\sigma_1(\lambda)G(\lambda), \quad I_{2e} = \sum_{\lambda=0}^{A} F(\lambda)\sigma_2(\lambda)G(\lambda),$$
$$I_{3e} = \sum_{\lambda=0}^{A} F(\lambda)\sigma_3(\lambda)G(\lambda), \tag{A.7}$$

$F(\lambda)$ is the intensity of the solar EUV flux radiation at a specified wavelength λ. The photoionization crossections σ_1, σ_2, and σ_3 for atomic oxygen with the formation of $O^+(^4S), O^+(^2D)$, and $O^+(^2P)$ ions have been presented by Richards et al. (1994a), where the correction factor $G(\lambda) = 0.8 \, (A/\lambda - 1)$, $A = 56.3$ nm, and $K_1 - K_7$ are the rate coefficients of the chemical reactions displayed in

Table 2. In Eqs. A.1-A.3 the values of $[O], [O_2], [N_2], T_n, T_e, T_i, T_v$, and W are taken at h_0 altitude. We take into account the input of $O^+(^2D)$ and $O^+(^2P)$ ions without including the reaction of $O^+(^2D)$ and $O^+(^2P)$ ions with electrons, and assume that $I \approx$ const.

Let us compare the disturbed NmF2(d), hmF2(d) with the undisturbed NmF2(q), hmF2(q). If we consider that

$$T_i = T_n, v_{in} = \text{const}\sqrt{T_n} \, [O], \tag{A.8}$$

and the values of C_f, I, Vf_1, f_2, and f_3V are about the same for both the undisturbed period and magnetic storm:

$$I(q) \exp[V(q) \, f_1(q)] \approx I(d) \exp[V(d)f_1(d)], \tag{A.9}$$

$$|T_n(d)\ln f_0(d) - T_n(q)\ln f_0(q)| >> |f_2(d) +$$
$$f_3(d)V(d) - f_2(q) + f_3(q)V(q)|, \tag{A.10}$$

then

$$\text{NmF2}(d)/\text{NmF2}(q) = a(d)/a(q), \tag{A.11}$$

$$\text{hmF2}(d) - \text{hmF2}(q) = 1.92 \cdot 10^{-2}$$
$$[T_n(d)\ln f_0 \, (d) - T_n(q) \ln f_0(q)], \tag{A.12}$$

where $a = \{[O]^2/L\}^{2/3}\sqrt{T_n}$.

If also

$$L \approx \text{const} \, [N_2](T_n)^2, T_n(d) \approx T_n(q) = T, \tag{A.13}$$

then

$$\text{foF2}(d)/\text{foF2}(q) = A(d)/A(q), \tag{A.14}$$

$$\text{hmF2}(d) - \text{hmF2}(q) = 1.92 \cdot 10^{-2} \, T \ln[B(d)/B(q)], \tag{A.15}$$

where foF2 is the critical frequency of the F2 layer peak, $A = (T_n)^{-5/12}\{[O]^2/[N_2]\}^{1/3}$, $B = [O][N_2](T_n)^{3.5}$.

The Eqs. A.14-A.15 with the same value of the B coefficient but another value of $A = \{(T_n)^{-2}[O] \, /[N_2]^{16/28}\}^{0.65}$ were used by Kishcha (1995) to describe the foF2 and hmF2 variations during several magnetic storms. Substorm effects were taken into account by Kishcha (1995) using a simple analytical description.

There is absolutely no reason to assert that conditions of Eqs. A.9-A.11 are valid during all storms, but during some storms Eqs. (A.14)-(A.15) may be valid with some small errors. The results presented in this paper show that the algorithm used by Kishcha (1995) gives satisfactory agreement between the measured NmF2(d)/NmF2(q) and hmF2(d)-hmF2(q) and the calculated NmF2(d)/NmF2(q) and hmF2(d)-hmF2(q) during the March and April storms, though often results differ greatly from the measured NmF2 and hmF2.

Equation A.2 can also be used in the method developed by Richards (1991) to calculate an equivalent neutral wind from the the hmF2 measurements. In this method the equivalent neutral wind at the next time-step

$$U(t + \Delta t) = (h_{\text{exp}}(t + \Delta t) - h'(t))/\alpha(t) + U'(t), \tag{A.16}$$

Reaction	Rate coefficient	Reference
$O^+(^2D)+O \rightarrow O^+(^4S)+O$,	$K_1 = 10^{-10}$ cm^3 s^{-1}	Fox and Dalgarno (1985)
$O^+(^2P)+O \rightarrow O^+(^4S)+O$,	$K_2 = 4 \cdot 10^{-10}$ cm^3 s^{-1}	Chang et al. (1993)
$O^+(^2P)+N_2 \rightarrow O^+(^4S)+N_2$,	$K_1 = 3.4 \cdot 10^{-10}$ cm^3 s^{-1}	Chang et al. (1993)
$O^+(^2P) \rightarrow O^+(^4S)+h\nu$,	$K_4 = 0.047$ s^{-1}	Seaton and Osterbrock (1957)
$O^+(^2P) \rightarrow O^+(^4D)+h\nu$,	$K_5 = 0.172$ s^{-1}	Seaton and Osterbrock(1957)
$O^+(^2D) +N_2 \rightarrow N_2^+ +O$,	$K_6 = 8 \cdot 10^{-10}$ cm^3 s^{-1}	Johnsen and Biondi (1980)
$O^+(^2D) +O_2 \rightarrow O_2^+ +O$,	$K_7 = 7 \cdot 10^{-10}$ cm^3 s^{-1}	Johnsen and Biondi (1980)
$O^+(^2P)+e \rightarrow O^+(^4S)+e$,	$K_8 = 4.7 \cdot 10^{-8} \, (300/T_e)^{0.5}$ cm^3 s^{-1}	Torr and Torr (1982)
$O^+(^2D)+e \rightarrow O^+(^4S)+e$,	$K_9 = 7.8 \cdot 10^{-8} \, (300/T_e)^{0.5}$ cm^3 s^{-1}	Torr and Torr (1982)

Table 2. Chemistry of metastable ions

where $h_{exp}(t + \Delta t)$ is the measured F2-layer peak altitude at time $t + \Delta t$, $h'(t)$ and $U'(t)$ are the calculated heights of the F2 layer and the equivalent neutral wind at time t.

The value of $\alpha(t)$ is determined by modeling the diurnal variation of the F region as

$$\alpha(t) = (h_1(t) - h_2(t))/U_1(t) - U_2(t). \qquad (A.17)$$

Where $h_1(t)$ is the calculated height of the F2-layer peak for $U = U_1(t)$ at time t and $h_2(t)$ is the calculated height of the F2-layer peak for $U = U_2(t)$ at time t, subscripts 1 and 2 refer to two separate model calculations at time t with the input parameters $U = U_1(t)$ and $U = U_2(t)$.

$$W(t + \Delta t) = (h_{exp}(t + \Delta t) - h'(t))/\beta(t) + W'(t), \qquad (A.18)$$

$$\beta(t) = (h_1(t) - h_2(t))/(W_1(t) - W_2(t)), \qquad (A.19)$$

where $h'(t)$ and $W'(t)$ are the calculated heights of the F2 layer and the equivalent drift velocity of the plasma at time t, $h_1(t)$ and $h_2(t)$ are the calculated heights of the F2-layer peak for $W = W_1(t)$ and $W = W_2(t)$. In this case, from Eq. A.2 it follows that

$$\beta(t) = \frac{\partial}{\partial W} hmF2 = 1.67 \cdot 10^{-5} f_3 (T_n v_{in})^{2/3} L^{-1/3}, \qquad (A.20)$$

where the values of f_3, T_n, v_{in}, and L are given at 300-km altitude (the dependence of β on altitude is small at the F-region altitudes because of $\beta(t) \sim \{[O]^2/L\}^{1/3}$).

Note that approximation Eq. A.2 is valid only during a quiet daytime period. But from our calculations we found that the use of Eqs. A.18, A.20 gives hmF2 to sufficient accuracy during daytime and nighttime quiet and disturbed periods. The reason for this conclusion is that the values of $\alpha(t)$ and $\beta(t)$ do not have to be known precisely (Richards, 1991)

We often do not have the observed hmF2 and thus cannot use the method developed by Richards (1991) or our modification Eqs. A.18, A.20 to calculate an equivalent plasma drift velocity. To overcome this problem, we can try to use hmF2$_{IRI}$ given by the IRI-90 model (Bilitza, 1990) to calculate an equivalent plasma drift velocity, W_{IRI}, for some hypothetical undisturbed conditions with the same solar and time conditions as during the studied geomagnetic storm:

$$W_{IRI}(t + \Delta t) = (hmF2_{IRI}(t + \Delta t) - hmF2(t))/\beta(t) + W_{IRI}(t), \qquad (A.21)$$

where hmF2(t) and $W_{IRI}(t)$ are the calculated heights of the F2 layer and the equivalent drift velocity of the plasma at time t, and the value of $\beta(t)$ is calculated from Eq. A.20.

After that we calculate the wind-induced plasma drift velocities

$$W_q = U_\Theta(q)\cos I, \quad W_d = U_\Theta(d)\cos I, \qquad (A.22)$$

where U_Θ is the component of the thermospheric wind for quiet (q) or disturbed (d) conditions in spherical polar coordinates (r, Θ, Φ), r denotes radical distance from the Earth's center Θ is the geomagnetic colatitude, ϕ is the geomagnetic longitude, I is the magnetic field dip angle and $U_\Theta(q)$ and $U_\theta(d)$ are obtained by solving two momentum equations for the horizontal components of thermospheric wind (Pavlov, 1994).

Finally, the plasma drift velocity in the ion continuity equations is given by Pavlov (1995) as

$$W = W_d - W_q + W_{IRI}. \qquad (A.23)$$

References

Abdou, W. A., D. G. Torr, P. G. Richards, M. R. Torr, and E. L. Breig, Results of a comprehensive study of the photochemistry of N_2^+ in the ionosphere, *J. Geophys. Res.*, **89**, 9069 -9079, 1984.

Albritton, D. L., I. Dotan W. Lindinger, M. Mc Farland, J. Tellinghuisen, and F. C. Fehsenfeld, Effects of ion speed distribution in flow-drift tube studies of ion-neutral reactions, *J. Chem. Phys.*, **66**, 410–421, 1977.

Badin, V. I., Analytical dependencies of the electron density and peak height of the daytime F2 layer on plasma drift velocity and other parameters of the atmosphere, (in Russian) *Geomagn. Aeron.*, **29**, 795-798, 1989.

Badin, V. I., and M. G. Deminov, Plasma drift effect on the F2-region ionospheric structure (in Russian) in *Ionospheric forecast,* Eds. R. A. Zevakina and N. P. Sergienko, *Nauka, Moscow*, pp 79-81, 1982.

Banks, P. M., Collision frequencies and energy transfer electrons, *Planet. Space Sci.*, **14**, 1085-1090, 1966.

Biltza D., Progress report on IRI status, *Adv. Space Res.*, **10**, (11),3-(11),5, 1990.

Buonsanto, M. J., Seasonal variations of day-time ionisation flows inferred from a comparison of calculated and observed NmF2, *J. Atmos, Terr. Phys.*, **48**, 365–373, 1986.

Buonsanto, M. J., J. C. Foster, and D. P. Sipler, Observations from Millstone Hill during the geomagnetic disturbances of March and April 1990, *J. Geophys. Res.*, **97,** 1225–1243, 1992a.

Buonsanto, M. J., Y. K. Tung, and D. P. Sipler, Neutral atomic oxygen density from nighttime radar and optical wind measurements at Millstone Hill, *J. Geophys. Res.*, **97,** 8673–8679, 1992b.

Buonsanto, P. G. Richards, W. K. Tobiska, S. C. Solomon, Y. -K. Tung, and J.A.Fennelly, Ionosperic electron densities calculated using different EUV flux models and cross-sections: comparison with radar data, *J. Geophys. Res.*, **100** 14569–114580, 1995.

Burnside, R. G., C. A. Tepley, and V. B. Wickwar, The $O^+ - O$ collision cross-section: can it be inferred from aeronomical measurements? *Ann. Geophysicae*, **5**, 343–350, 1987.

Chang, T., P. G. Richards, and D. G. Torr, Reevaluation of the $O^+(^aP)$ reaction:rate coefficients derived from Atmosphere Explorer C observation, *J. Geophys. Res.*, **98**, 15589–15597, 1993.

Chen, A., R. Johnsen, and M. A. Biondi, Measurements of the $O^+ + N_2$ and $O^+ + O_2$ reactions rates from 300 to 900 K, *Chem. Phys.*, **69**, 2688–2691, 1978.

Davis, C. J., A. D. Farmer, and A. Aruliah, An optimised method for calculating the $O^+ - O$ collision parameter from aeronomical measurements, *Ann. Geophysicae*, **13**, 541–550, 1995.

Ferguson, E. E., comment on "The effect on the thermospheric chemistry of a resonant charge-exchange reaction involving vibrationally exicited N_2^+ ions with atomic oxygen" by W.A. Abdou *et al.*, *J. Geophys. Res.*, **89**, 399–400, 1984.

Foster, J. C., M. J. Buonsanto, M. Mendillo, D. Nottingham, F. C. Rich, and W. Denig, Coordinated stable auroral red arc observations: relationship to plasma convection, *J. Geophys. Res.*, **99**, 11429–11439, 1994.

Fox, J. L. and A. Dalgarno, The vibrational distribution of N_2^+ in the terrestrial ionosphere, *J. Geophys. Res.,* **90,** 7557–7567, 1985

Hedin, A. E., MSIS-86 thermospheric model, *J.Geophys. Res.*, **92**, 4649– 4662, 1987.

Johnsen, R., and M. A. Biondi, Laboratory measurements of the $O^+(^2D) + N_2$ and $O^+(^2D) + O_2$ reaction rate coefficients and their ionospheric implications, *Geophys. Res. Lett.*, **7,** 401–403, 1980.

Kashirin., A. I., Photoionization in the night-time ionosphere (in Russian) *Geomagn. Aeron.,* **26,** 563–568, 1986.

Kishcha, P. V., Indices and updating procedures for modeling of ionospheric disturbances, *Adv. Space Res.*, **16,** 55–64, 1995.

Krinberg, I. A., *Electron kinetics in the earth's ionosphere and plasmasphere* (in Russian) Nauka, Moscow, 1978.

Krinberg, I. A. and A. V. Tashchilin, Refilling of geomagnetic force tubes with a thermal plasma after magnetic disturbance, *Ann. Geophysicae*, 38, 25–32, 1982.

Krinberg, I. A., and A. V. Tashchilin, *Ionosphere and plasmasphere*, (in Russian) Nauka, Moscow, 1984.

Miller, K. L., D. G. Torr, and P. G. Richards, Meridional winds in the thermosphere derived from measurements of F2-layer height, *J. Geophys. Res.*, **91,** 4531–4538, 1986.

Moffett, R. J., R. Sellek, and G. J. Balley, The influence of $O^+ - O$ collision frequency on ionospheric F-region behaviour, *J. Atmos. Terr. Phy.*, **52,** 125–132, 1990.

Newton, G. P., J. C. G. Walker, and P. H. E. Meijer, Vibrationally excited nitrogen in stable auroral red arcs and its effect on ionospheric recombination, *J. Geophys. Res.*, **79,** 3807–3818, 1974.

Oppenheimer, M., E. R. Constantinides, K. Kirby - Docken, G. A. Victor, and A. Dalgarno, Ion photochemistry of the thermosphere from Atmosphere Explorer C measurements, *J. Geophys. Res.*, **82,** 5485–5492, 1977.

Pavlov, A. V., Possible accuracy of theoretical forecasts of the major ionospheric parameters, in *Forecast of disturbances in the ionosphere and magnetosphere and solar activity* (in Russian), Eds. R. A. Zevakina and V. N. Obridko, Nauka, Moscow, pp 177–192, 1987.

Pavlov, A. V., The role of vibrationally excited nitrogen in the ionosphere, *Pure Appl. Geophys.*, **127,** 529–544, 1988.

Pavlov., A. V., About the role of vibrationally excited nitrogen in the sabauroral red arc region (in Russian), *Geomagn. Aeron.*, **29,** 948–953, 1989.

Pavlov, A. V., The role of vibrationally excited nitrogen in the formation of the mid-latitude ionisation trough,, *Ann. Geophysicae*, **11,** 479–484, 1993.

Pavlov, A. V., The role vibrationally excited nitrogen in the formation of the mid-latitude ionospheric storms, *Ann. Geophysicae*, **12,** 554–564, 1994.

Pavlov, A. V., Mechanisms of the electron density depletion in the SAR arc region, *Ann. Geophysicae*, **14,** 211–221, 1996.

Pavlov, A. V., and A. A. Namgaladze, Vibrationally excited nitrogen in the upper atmosphere. Review paper (in Russian) *Geomagn. Aeron.*, **28,** 705–721, 1988.

Pesnell, W. D., Momentum transfer collision frequency of O^+ –O, *Geophys. Res. Lett.*, **20,** 1343–1346, 1993.

Raitt, W. J, Schunk R. W., and P. M. Banks, Ionospheric composition in SAR-arcs, *Planet. Space Sci.*, **24,** 105–114, 1976.

Reddy, C. A., W. R. Hoegy, W. D. Pesnell, H. G. Mayr and C. O. Hines, Accuracy of O^+−O collision cross-section deduced from ionosphere-thermosphere observations, *Geophys. Res. Lett.*, **21,** 2429–2432, 1994.

Richards, P. G., An improved algorithm for determining neutral winds from the height of the F2 peak electron density, *J. Geophys. Res.*, **96,** 17839–17846, 1991.

Richards, P. G., and P. G. Torr, A factor of 2 reduction in theoretical F2 peak electron density due to enhanced vibrational excitation of N_2 in summer at solar maximum, *J. Geophys. Res.*, **91,** 11331–1336, 1986.

Richards, P. G., D. G. Torr, and W. A. Abdou, Effects of vibrational enhancement of N_2 on the cooling rate of ionospheric thermal electrons, *J. Geophys. Res.*, **91,** 304–310, 1986.

Richards, P. G., J. A. Fennelly, and D. G. Torr, EUVAC : A solar EUV flux model for aeronomical calculations, *J. Geophys. Res.*, **99,** 8981–8992, 1994a.

Richards, P. G., D. G. Torr, M. J. Buonsanto and D. P. Sipler, Ionospheric effects of the March 1990 magnetic storm: comparison of theory and measurements, *J. Geophys. Res.*, **99,** 23359–23365, 1994b.

Rodger, A. S., Moffett R. J. , and S. Quegan, The role of ion drift in the formation of ionization troughs in the mid- and high-latitude ionosphere - a review, *J. Atmos. Terr. Phys.*, **54,** 1–30, 1992.

Salah, J. E., Interim standard for the ion-neutral atomic oxygen collision frequency, *Geophys. Res. Lett.*, **20,** 1543–1546, 1993.

Schmeltekopf, A. L., E. E. Ferguson, and F. C. Fehsenfeld, Afterglow studies of the reactions He^+, $He(2^3 S)$, and O^+ with vibrationally excited N_2, *J. Chem. Phys.*, **48,** 2966–2973, 1968.

Schunk, R. W., W. J. Raitt and P. M. Banks, Effect of electric fields on the daytime high-latitude E and F region, *J. Geophys. Res.*, **80,** 3121–3130, 1975.

Seaton, M. J., and D. W. Osterbrock, Relative OII intensities in gaseous nebulae, *Astrophys. J.*, **125,** 66–83, 1957.

Sipler, D. P, M. E. Hagan, M. E. Zipf and M. A. Biondi, Combined optical and radar wind measurements in the F region over Millstoun Hill, *J. Geophys. Res.*, **96,** 21255–21262, 1991.

St.-Maurice, J. -P., and D. G. Torr, Nonthermal rate coefficients in the ionosphere: The reaction of O+ with N_2, O_2 and NO, *J. Geophys. Res.*, **83,** 969–977, 1978.

Tobiska, W. K., The empirical solar EUV irradiance model EUV94 (abstract), *EOS Trans. AGU*, **74(43),** Fall Meeting suppl., 490, 1993.

Tobiska, W. K., Modeled soft X-ray solar irrradiance, *Sol. Phys.*, **152,** 207–215, 1994.

Torr, M. R., and D. G. Torr, The role of metastable species in the thermosphere, *Rev. Geophys. Space Phys.*, **20,** 91–144, 1982.

Torr, M., R. D. G. Torr, P. G. Richards, and S. P. Yung, Mid-and low-latitude model of thermospheric emissions. 1. $O^+(^2P)$ 7320 A and $N_2(^2P)$ 3371 A, *J. Geophys. Res.*, **95,** 21147–21168, 1990.

Van Zandt, T. E., and T. F. O'Malley, Rate coefficient for the reaction of O^+ with vibrationally excited N_2, *J. Geophys.Res.*, **78,** 6818–6820, 1973.

Viehland, L. A., and E. A. Mason, Statistical - mechanical theory of gaseous ion-molecule reaction in an electrostatic field, *J. Chem. Phys.*, **66,** 422–434, 1977.